NAL TR-268T

UDC 533.697:
533.662.3:
621.454

TECHNICAL REPORT OF NATIONAL AEROSPACE LABORATORY

TR-268T

Aerodynamic Design and Test Results of Front Fans

Shoichi FUJII, Hideo NISHIWAKI, Mitsuo GOMI

January 1972

NATIONAL AEROSPACE LABORATORY

CHŌFU, TOKYO, JAPAN

List of NAL Technical Reports

TR-241	Full-Scale Fatigue Test of YS-11A-500/600 Turboprop Transport Wing (I Safe life Fatigue Test Loads and Test Method)	Kazuyuki TAKEUCHI, Toshio NOHARA & Hiroo ASADA	July 1971
TR-242	Measurement of three-dimensional mean Velocity Vector and Reynolds Stress by Single Rotatable Hot-wire	Yoshio HAYASHI, Teruomi NAKAYA	July 1971
TR-243	A Method for the Calculation of Lifting Potential Flow Problems —Part 1— Theorotical Basis	Masao EBIHARA	July 1971
TR-244	Measurements of Dynamic Stability Derivatives in Supersonic Blowdown Wind Tunnel	Kazuaki TAKASHIMA, Seizo SAKAKIBARA & Hideo SEKINE	July 1971
TR-245	An Analytical Method to Predict Height-Velocity Diagram Critical Decision Point of Rotorcraft	Masaki KOMODA	Aug. 1971
TR-246	On Analysis of Large Deformation Problems of Beam	Hideo Izumi	Nov. 1971
TR-247	On the theory of Free Streamlines Past an Arbitrary Shape	Hitoshi TAKAHASHI	Sep. 1971
TR-248	A Description of the Ideas Underlying a Computer Programme for Predicting the Aerofoil Pressure Distributions in Subcritical Viscous Flow	Masao EBIHARA, Youji ISHIDA & Tokio OKONOGI	Nov. 1971
TR-249	Modified Optimization Algorithm for Computer Storage Problems in Generalized Newton-Raphson Method	Toru SHIHO	Oct. 1971
TR-250	Large Deflection of Cantilever Beams	Yasuo TADA, Kazuo KUSAKA	Oct. 1971
TR-251	Inertial Force Field Due to Nutational Motion of Spinning Axi-symmetric Satellite and Its Application to Nutation Damper	Chikara MURAKAMI, Yoshiaki OHKAMI	Nov. 1971
TR-252 T	A Study of Subsonic, Two-Dimensional Wall-Interference Effect in a Perforated Wind Tunnel with Particular Reference to the NAL 2m×2m Transonic Wind Tunnel — Inapplicability of the Conventional Boundary Condition	Masao EBIHARA	Dec. 1971
TR-253	A Calculation of Profile Drag of Airfoils in Compressible Flow	Youji ISHIDA	Nov. 1971
TR-254	Interference Between Wing and Surface of Velocity Discontinuity	Norio INUMARU	Nov. 1971
TR-255	The Study on the Motion of an Artificial Satellite in the Earth's Gravitational Field	Sumio TAKEUCHI, Koichi MATSUSHIMA	Dec. 1971
TR-256	On the Aerodynamic damping moment in Pitch of a Rigid Helicopter Rotor in Hovering	Kingo TAKAZAWA	Nov. 1971
TR-257	The Dynamic Stability of a Connected Rod under Periodic Longitudinal Force	Masaaki SANO	Jan. 1972

Aerodynamic Design and Test Results of Front Fans*

By Shoichi FUJII**, Hideo NISHIWAKI** and Mitsuo GOMI**

SUMMARY

Full scale front fans were designed and tested with satisfactory results. The flow field in passing through the fans was estimated with a powerful method called streamline-curvature technique, and the first test-program was carried out in equipping the rotor blade row without snubbers (part-span shroud) and the second conducted with them. A comparison of both experimental data enabled the flow behavior and aerodynamic characteristics to be visualized under these two different inlet conditions.

NOMENCLATURE

B.P.R.	bypass ratio
c	chord length
c_1	constant determined by continuity
c_p	specific heat at constant pressure
D	diffusion factor
G	weight flow
g	acceleration of gravity
H	total enthalph
$\bar{H}$	Pitot tube calibration constant
H_z	shape factor in axial direction
i	incidence angle
J	mechanical-to-thermal energy conversion factor
J_n	first kind Bessel function of nth order ($n=0, 1, 2, \cdots\cdots$)
j_n	roots of $J_1(j_n)=0$
K	constant used for evaluating deviation angles
M	Mach number
m	streamline projected on a meridian surface
m_0	strength of point source
(n, m)	(station number, radial point)
N/N^*	(Corrected rotative speed)/(Designed rotative speed)
$P(r)$	function of radius, r
p	static pressure
P	total pressure
$Q(r)$	function of radius, r
(r, θ, z)	cylindrical coordinate system
r_c	radius of curvature of meridian projection curve, m
R	gas constant
S	entropy
T	static temperature
U	uniform velocity or peripheral speed
U_p	axial velocity with shroud removed
V	velocity
VR	axial-velocity ratio across a blade row
Z	z/r_t=(abscissa along axis of center body)/(tip radius)
$\boldsymbol{V}$	velocity vector
∇	gradient
λ	angle between meridional velocity, V_m and axial velocity, V_z
ρ	density
κ	ratio of specific heats
$\bar{\omega}$	total pressure loss coefficient
σ	solidity
ϕ	stream function
π or π_0	total pressure ratio or the ratio of the circumference to its diameter
θ/c	loss parameter
α	absolute flow angle
β	relative flow angle
δ^*	displacement thickness
θ	momentum thickness
y	radial coordinate, the origin being the point at which the snubber wake begins
ν	radius ratio (r/r_t)
δ	deviation angle
ε	turning angle
η	adiabatic efficiency

* Received December 21, 1971

** Aero-Engines Division

Subscripts

i	inlet to a blade row
l	left side
r	radial direction or rotor or right
s	stator
m	meridian
n	$n=1, 2, 3, \cdots\cdots$
T	traverse
t	tip
h	hub
des.	design
z	axial direction
0	stagnation or station upstream inlet strut
1	before rotor blades
2	behind rotor
3	behind stator blades
θ	circumferential direction
$-\infty$	infinitely upstream
or	orifice

Superscripts

'	relative
*	design or displacement

INTRODUCTION

Most of modern jet engines have been equipped with front fans, mainly because of necessity of raising the mass flow rate which can be converted into the engine thrust and, in turn, of obtaining a better propelling efficiency.

Therefore, a component research regarding the front fan had been put forward. The full scale front fans having 940 mm inlet diameter were then designed and tested in order to pursue investigations into both aspects of aerodynamic and mechanical design technology.

As to the aerodynamic design, there were several problems yet to be solved; operation of rotor blades in a high-speed flow: a steep slope in the radial distribution of enthalpy rise across a rotating blade row (which might cause a highly three-dimensional flow): effects of spinner shape and contour on the streamline displacement. Thus, an attempt was made with the aid of a large scale computing facility to incorporate the streamline displacement and curvature terms into the design calculation for evaluating the internal flow movement across each blade row. As another design problem, it was apparently known that snubbers (or sometimes called a part-span shroud) were almost inevitable in the conventional-alloy front fan subjected to a severe inlet distortion. Nevertheless, since we had no reasonable technique of estimating the effect of snubbers itself on the flow pattern, two fan rotors with and without snubbers were planned and tested, without any additional design consideration taken into the disturbance caused in a flow field due to the presence of snubbers.

The performance comparison for both cases was then carried out in analyzing the detailed experimental data, making use of streamline-curvature computing procedure again for the reduction of the internal-flow survey data. Hence, a new approach was shown to express the local cascade performance along its span, instead of a usual blade-element concept.

Description about the technology of manufacturing a snubbered blade, the measurement record of alternating stresses of rotating blades, and sound level captured in the neighbor of the test vehicle were not presented in this paper, although some structural and aerodynamic considerations on snubber position and shape were given briefly.

AERODYNAMIC DESIGN

Three dimensional compressible flow-equation

The equation of motion for the inviscid, steady compressible flow without body-force can be written in a vector form coupling with some thermodynamic relations

$$-\boldsymbol{V}\times\nabla\times\boldsymbol{V}=-\nabla H+T\nabla S \qquad (1)$$

Applying the cylindrical coordinates system (r, θ, z) to Eq. (1) resolves into scalar forms; as the component of radial direction, we have

$$Jg\frac{\partial H}{\partial r}=JgT\frac{\partial S}{\partial r}+\frac{V_\theta}{r}\frac{\partial(rV_\theta)}{\partial r}+V_z\frac{\partial V_z}{\partial r}-V_z\frac{\partial V_r}{\partial z} \qquad (2)$$

Referring to Fig. 1 where a streamline is projected on the plane r–z as a curve m, the last

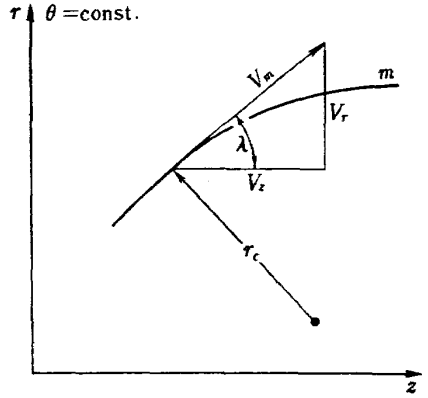

Fig. 1 Axi-symmetric flow

term of right hand side of Eq. (2) is expressed, by making use of the relation $V_r = V_z \tan\lambda$.

$$V_z \frac{\partial V_r}{\partial z} = V_r \frac{\partial V_z}{\partial z} + \frac{V_z^2}{\cos^3\lambda} \cdot \frac{1}{r_c} \qquad (3)$$

The term $\partial V_z/\partial z$ appearing in Eq. (3) is considered to be of small order except for flow region near a singular point. In addition, since V_r is much smaller than V_z in the usual axial turbomachines, Eq. (3) may be approximated such that

$$V_z \frac{\partial V_r}{\partial z} \cong \frac{V_z^2}{\cos^3\lambda} \cdot \frac{1}{r_c} \left(= V_z^2 \frac{\partial}{\partial z} \tan\lambda \right) \qquad (4)$$

Putting Eq. (4) back into Eq. (2) and rearrangement gives

$$\frac{\partial V_z^2}{\partial r} - \left\{ \frac{2}{r_c \cos^3\lambda} + \frac{1+(dr/dz)^2}{c_p} \left(\frac{\partial S}{\partial r} \right) \right\} V_z^2 = 2gJ \left\{ c_p \frac{\partial T_0}{\partial r} - \left(T_0 - \frac{V_\theta^2}{2gJc_p} \right) \left(\frac{\partial S}{\partial r} \right) \right\} - 2 \frac{V_\theta}{r} \frac{\partial (rV_\theta)}{\partial r} \qquad (5)$$

For convenience, if the coefficients of V_z^2 would be considered as functions of r alone, we can perform the integration of Eq. (5) to produce

$$V_z^2 = c_1^2 e^{-\int P(r)dr} + e^{-\int P(r)dr} \int e^{\int P(r)dr} Q(r)\, dr \qquad (6)$$

where

$$P(r) = -\left\{ \frac{2}{r_c \cdot \cos^3\lambda} + \frac{1+(dr/dz)^2}{c_p} \left(\frac{\partial S}{\partial r} \right) \right\} \qquad (7)$$

$$Q(r) = 2gJ \left\{ c_p \frac{\partial T_0}{\partial r} - \left(T_0 - \frac{V_\theta^2}{2gJC_p} \right) \cdot \left(\frac{\partial S}{\partial r} \right) \right\} - 2 \frac{V_\theta}{r} \frac{\partial (rV_\theta)}{\partial r} \qquad (8)$$

and the constant c_1 is determined by the condition of continuity*

$$G = 2\pi \int_{r_h}^{r_t} g\rho V_z r\, dr \qquad (9)$$

As Eqs. (7) and (8) stand, expression of partial derivatives with respect to r such as $\partial S/\partial r$, $\partial T_0/\partial r$, etc. are seen. This fact means that the effect of the derivatives with respect to z such as $\partial S/\partial z$, $\partial T_0/\partial z$, etc. on the computed profile of V_z should be taken into consideration as well as the influence of the derivatives with respect to r. The streamline curvature technique will be then one of most powerful calculation methods in the situation treated herein.

* If the lower limit of the integral of Eq. (6) is taken as r_h, c_1 represents physically the axial velocity at $r = r_h$.

Streamline curvature technique

The desire to incorporate the streamline movement into the analyses of flow in turbomachines would be realized, to some extent, by a method called streamline curvature technique. In actual computation, however, the streamline shape is determined by connecting finite points which are assumed to be lying on a stearmline**. Therefore, the streamline curvature method will not give the 'exact' evaluation of streamline shape but the approximate estimation of streamline displacement at finite points, and hence the connection of these points yields the curvature which may directly relate to the evaluation of the term $1/r_c$ in Eq. (7).

Several methods of generating streamline from the connection of points were discussed in the literature [1]~[3]***. Among these methods, some comparisons of two fitting curves, that is, spline-fit [4] and least-mean-squares were made in our design problem. As a result, the approximate nature of spline-fit was not always applicable to solution on the digital computer. On the other hand, the least-mean-squares curve with six order terms, connecting 9~15 points, had a reasonable character of fitting curve from the authors' experience [5]. The practical procedure for designing the front fans is then described in the following.

As shown in Fig. 2, the calculation stations from 1st to nth were placed in the axial direction, and then the points used for defining streamline were radially chosen from 1st to $(m+1)$ th at every station. At the beginning, in fact, every point was located in a distance giving the equal annulus area between suc-

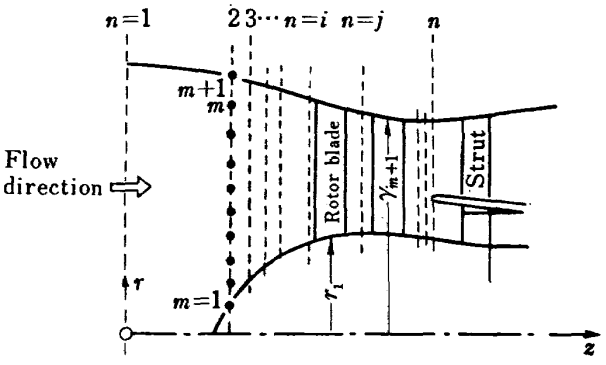

Fig. 2 Calculation stations

** The word 'streamline' hereafter is equivalent to the meridional projection curve m in Fig. 1.

*** Numbers in brackets designate References at end of paper.

cessive two points. In addition, it was assumed that the location of the points at the first and last (nth) stations was not subjected to change during the relocation process of other points situated at stations from 2nd to (n-1)th. Moreover, it was postulated that $V_\theta=0$, $\partial S/\partial r=0$ and $T_0=$const. in the region before the rotor blade row. For the station between the rotor and stator, the following simultaneous equations were utilized to obtain the values of V_θ, $\partial S/\partial r$ and T_0 by use of the estimated loss-coefficient $\bar{\omega}$ and expected total pressure ratio π_0 along a radius,

$$\bar{\omega}=\left[1+\frac{\kappa-1}{2}\cdot\frac{U^2}{\kappa gRT_0}\left\{1-\left(\frac{r_i}{r}^2\right)\right\}\right]^{(\kappa/\kappa-1)} \times\left[\frac{1-\pi_0(T_0/T_{0i})^{(-\kappa/\kappa-1)}}{1-\left(1+\frac{k-1}{2}M_i'^2\right)^{(-\kappa/\kappa-1)}}\right] \tag{10}$$

$$V_\theta=\frac{Jgc_p}{U}(T_0-T_{0i}) \tag{11}$$

$$\left(\frac{J}{R}\right)\frac{\partial S}{\partial r}=\frac{\partial}{\partial r}l_n\frac{(T_0/T_{0i})^{(\kappa/\kappa-1)}}{\pi_0}+\left(\frac{J}{R}\right)\frac{\partial S_i}{\partial r} \tag{12}$$

where suffix 'i' denotes the condition before a blade row. It is noted that the loss and work relationship, Eq. (10), contains the term $(r_i/r)^2$ representing the radial displacement of streamline across the blade row. To the flow leaving from the stator blades, Eqs. (10), (11) and (12) are also applicable by equating $M_1'=M_1$ (absolute Mach number entering stator) and $T_{01}=T_0$ (no temperature rise).

Thus, the first calculation of determining flow condition at every point assigned from stations $n=2$ to $(n-1)$ was made by use of the least-mean-squares curve fitting the points and also of Eqs. (6)$\sim$(12). And then the new location of the points for use in defining the streamline was referred to r_{N+1} by satisfying the continuity condition such that

$$N\left(\frac{G}{m}\right)=2\pi\int_{r_1}^{r_{N+1}}\rho g V_z r dr, \quad (N=1,2,\cdots m) \tag{13}$$

where r_1 and r_{m+1} giving the location of points along upper and lower boundaries were not changed. The similar procedure was carried out until the relocation of all points defined by r_{N+1} became insensitive to the iterative process. In Fig. 3 is shown an example of converging process of r_{N+1} at the inlet station of rotor blades for the value of $n=15$ and $m=20$ in the case of 6th order least-mean-squares. It is seen that iteration over about fifteen cycles gave the reasonable convergence.

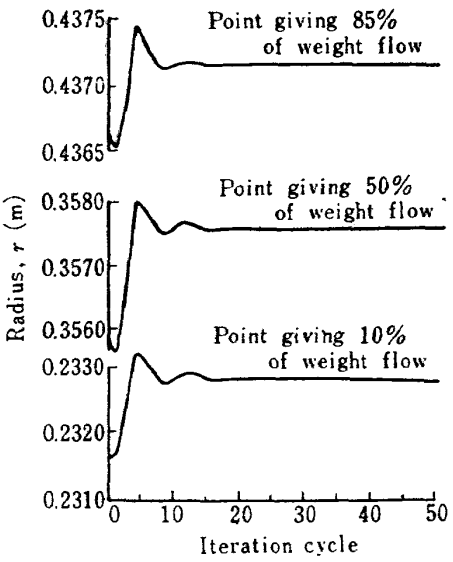

Fig. 3 Convergence of points defining streamline at rotor inlet station by computing cycles

In the Appendix A is described a comparison between the streamline curvature method and the exact solution made for the incompressible flow around a point source in an infinitely long duct of constant diameter.

Design philosophy

A series of the investigations of designing full scale front fans had started early in 1967. Based on the aerodynamic design technology concerning the transonic single and multi-stage-compressors which we had already finished testing at that time [6], [7], the velocity triangle and blading were selected. The inlet guide vanes were not installed in order to remove the noise generated by an interaction of shedding wakes from guided vanes with rotor blades. One of the most important factors we must have decided was 'Mach number' relative to a tip section of rotor blades. In general, the permissible Mach number would serve as playing an important role in prescribing the possible target performance such as a pressure ratio, mass flow rate, rotational speed, etc. Therefore, it was concluded from preliminary calculation that some conflicting factors accompanied with increasing Mach number might be expected to be compromised if the tip Mach number were within a value of approximately 1.25. On the other hand, the Mach number entering the stator blades was designed so as to be below the critical Mach number along the whole blade height because of our empirical fact that a combination of transonic rotor blade row with subsonic stator vanes would have a tendency to give a

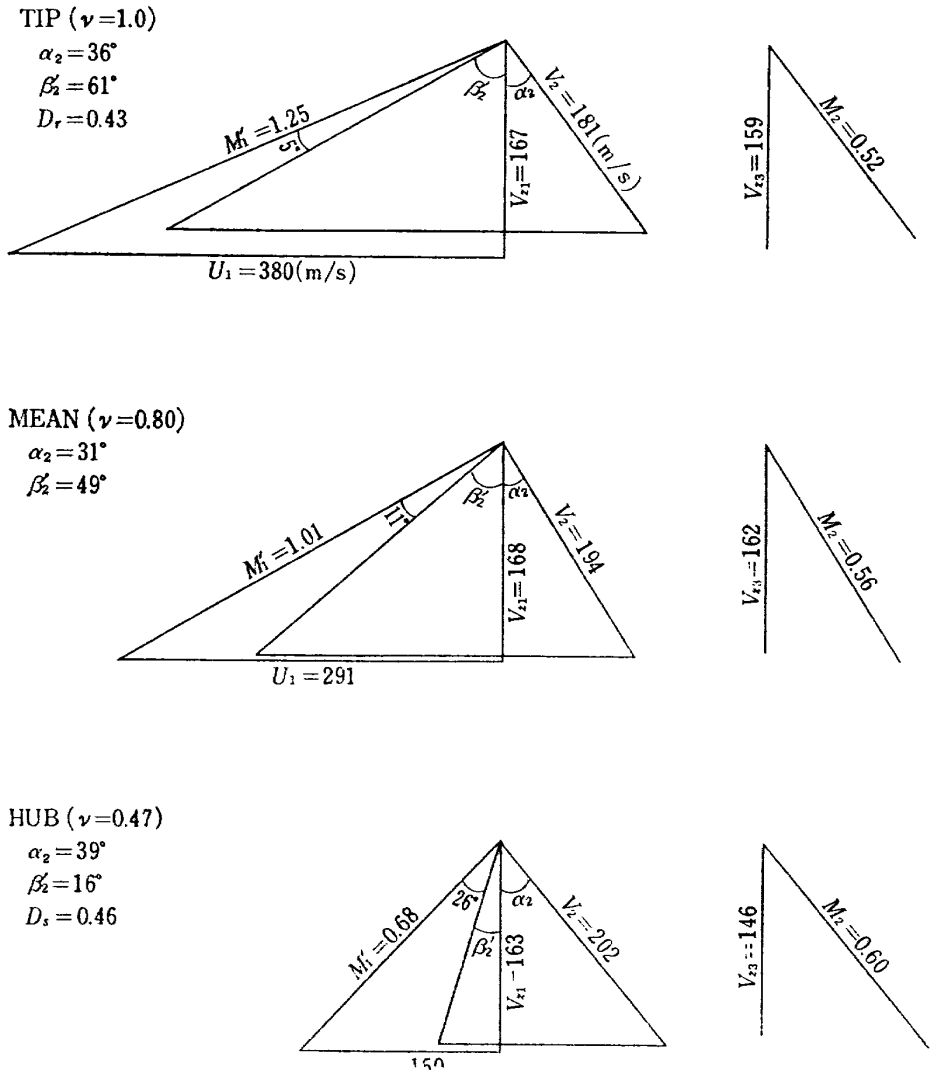

Fig. 4 Velocity triangles for the fan without snubbers

better performance, in comparison with high subsonic stator. Along with this line, the blade profiles were selected such that the double-circular-arc blade (D.C.A.) be for the rotor, the NACA 65-series-blade for the stator.

A mass flow rate and bypass ratio were mainly determined to meet the performance criteria of an actual engine which was planning to be equipped with the front fan investigated here, also considering capacity of the test facility for the fan component research.

Although the snubbers or part-span shroud were obviously necessary for practical use of the front-fan blades made of titanium alloy, there was no definite method for evaluating the effect of them on the aerodynamic performance. As a basis for obtaining further information about the snubbered blade design, therefore, the study program had been divided into two steps. The purpose of the first step was to determine the aerodynamic characteristics of the front fan without snubbers. The second was aiming at the test of the front fan with snubbers. The same test vehicle was utilized for both cases. The rotor blades with snubbers differed from those without snubbers in the number of blades and, hence, in the chord length and absolute thickness to satisfy the requirement that both rotor blades should have the same values of aerodynamic parameters such as the solidity, the thickness-chord ratio, and the camber and staggered angles.

The velocity triangles for the tip, mean and hub sections are presented in Fig. 4. Reviewing the experimental results of the reference [6], the root section of rotor blades was carefully designed in order to be operating below the critical Mach number in expectation of avoiding the performance deterioration due to

Table 1 a Rotor blading details

Radial position (r/r_t)	0.50 (Near hub)	0.70 (Mean)	0.94 (Near tip)
Camber angle (deg.)	18.4	10.3	7.3
Solidity	1.47	1.14	0.98
Stagger angle (deg.)	34.0	46.6	56.2
Thickness-chord ratio	0.069	0.035	0.035

Table 1 b Stator blading details

Radial position (r/r_t)	0.50 (Near hub)	0.70 (Mean)	0.94 (Near tip)
Camber angle (deg.)	42.2	38.4	41.9
Solidity	1.63	1.34	1.19
Stagger angle (deg)	14.8	13.3	13.4
Thickness-chord ratio	0.070	0.074	0.079

a high speed flow. On the solidity of the rotor tip section, which would relate directly to the magnitude of shock-loss and blade loading, it was imperative to employ the value of 0.90 as the permissible minimum in adjusting the aerodynamic and mechanical demands. We tried to keep the designed axial velocity ratio across a blade row within the value of 1.1~0.9, otherwise a higher or lower axial velocity ratio might involve some inaccuracies in the blading procedure. As shown in the figure the magnitude of Dr=0.43 and Ds=0.46 was settled as the diffusion factor for the rotor tip and stator hub sections respectively.

In the result, the target performance for the fan without snubbers was selected as follows; a mass flow rate to be entered through the fan inlet section having a diameter of 940 mm should be 104 kg/s at sea-level and at a rotational speed of 7770 rpm, with a pressure ratio of 1.34, an adiabatic efficiency of 84 per cent, and bypass ratio of 6.0.

The blading details for the rotor and stator blades are given in the Table 1(a) and (b).

AERO-AND MECHANICAL CONSIDERATIONS OF THE SNUBBERS

As mentioned before, the aerodynamic parameters of the rotor blades characteristic of solidity, camber angle, maximum thickness to chord ratio and stagger angle were maintained to be equal in both cases with and without snubbers. However, to shorten the blade spacing and hence a distance of snubber overhang from the airfoil surface, and also to keep the snubber root bending stress caused by the centrifugal force of the shroud within allowable level, the number of blades was increased from 25 to 33 in the case of the rotor blades with snubbers. Accordingly the aspect ratio increased from 2.65 to 3.50. Furthermore, the system supporting rotor-blades at the disk was changed from pin-jointed one to dove-tail type, corresponding to the change of vibrational movements due to the retaining action of the shroud.

The radial position of snubbers was determined as 64 per cent of blade span from the blade root so as to minimize the second-order bending mode of blade vibration and to suffice the requirement of enabling every blade of a row to be rotating in the same phase of first-order bending and torsional modes, respectively.

It is easily supposed that a thicker snubber will disturb the oncoming flow, make the blocked area and involved loss larger compared to thinner one. On the other hand, it should be understood that the bending stress at the snubber root will decrease in inverse proportion to a square of the thickness. Compromising these conflicting factors of aerodynamic and mechanical stipulation, then the absolute snubber thickness was chosen as 6.0 millimeter which would be equivalent to 2.5 per cent of mechanical annulus blockage, and the width selected as 40 per cent of the rotor-blade chord length that would amount to 20 per cent in the ratio of thickness to width. Both leading and trailing edges of snubbers were simply rounded getting a wider working range of the flow incidence angle due to the change of oncoming flow condition.

As a result, the gross weight of rotating parts with snubbered blades was reduced remarkably, compared to the case without snubbers. The adoption of higher aspect ratio (short chord-length) and much lighter root-joints was apparently the main source for such a weight reduction.

EXPERIMENTAL APPARATUS

A schematic drawing of the test facility is shown in Fig. 5. The test vehicle was driven by a gasturbine installed at the Aero-Engines Division of the National Aerospace Laboratory. The atmospheric air coming through an inlet silencer was led to the bellmouth of the fan to be tested. The compressed air in pass-

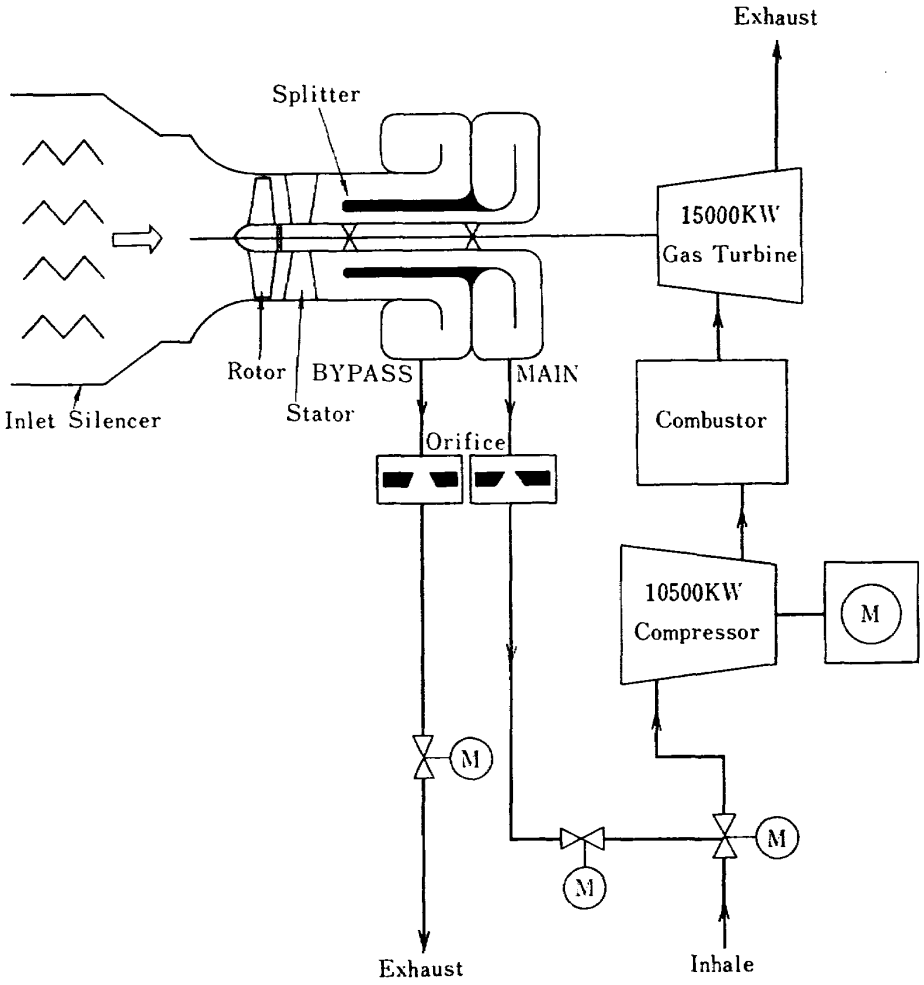

Fig. 5 Test facility and loop

ing through the blade row was divided at the outlet splitter into two portions; bypass and main air flows. The axial location of the splitter was set up in a distance more than one chord length of stator blade in order to avoid the performance deterioration due to the presence of the splitter very close to blade row. In addition, a rounded portion of splitter entrance was used for preventing probable local separation caused by a flow deviated from the designed value of bypass ratio. The amount of bypass and main air flows was measured independently by each orifice at the outlet and then the bypass air was exhausted through an outlet silencer, whereas the main air returned to the inlet of the gasturbine compressor. This recirculation system of main air was effectively used to change the ratio of bypass to main flow in order to simulate various operating conditions which would be encountered in an actual engine. While, the valve mounted in the downstream region of bypass flow conduit served as the main throttle for adjusting the over-all mass flow rate of the test fans.

The rotor blade for both cases with and without snubbers was made of titanium alloys in machinery-cutting, and stator blade was of stainless steels welded with the casing. The stator blade row was installed in one chord length of stator blades apart from the rotor blade row in order to reduce the noise due to the interaction of the blade rows.

INSTRUMENTATION

Each position of instruments is presented in Fig. 6. At the inlet section '0' where the area was large enough for the flow speed to be under 20 m/sec. even at the anticipated maximum flow rate, eight chromel-alumel thermocouples were placed for measuring the inlet stagnation temperature. To determine the inlet flow condition at section '1', firstly a three-hole cobra type yaw meter capable of being automatically balanced in flow direction was used for traversing flow passage from hub to tip blade sections, at some of all operating points tested. Second, at the other operating points no traversing was carried out to get the inlet flow condition. Namely, the static and total pressure along the blade

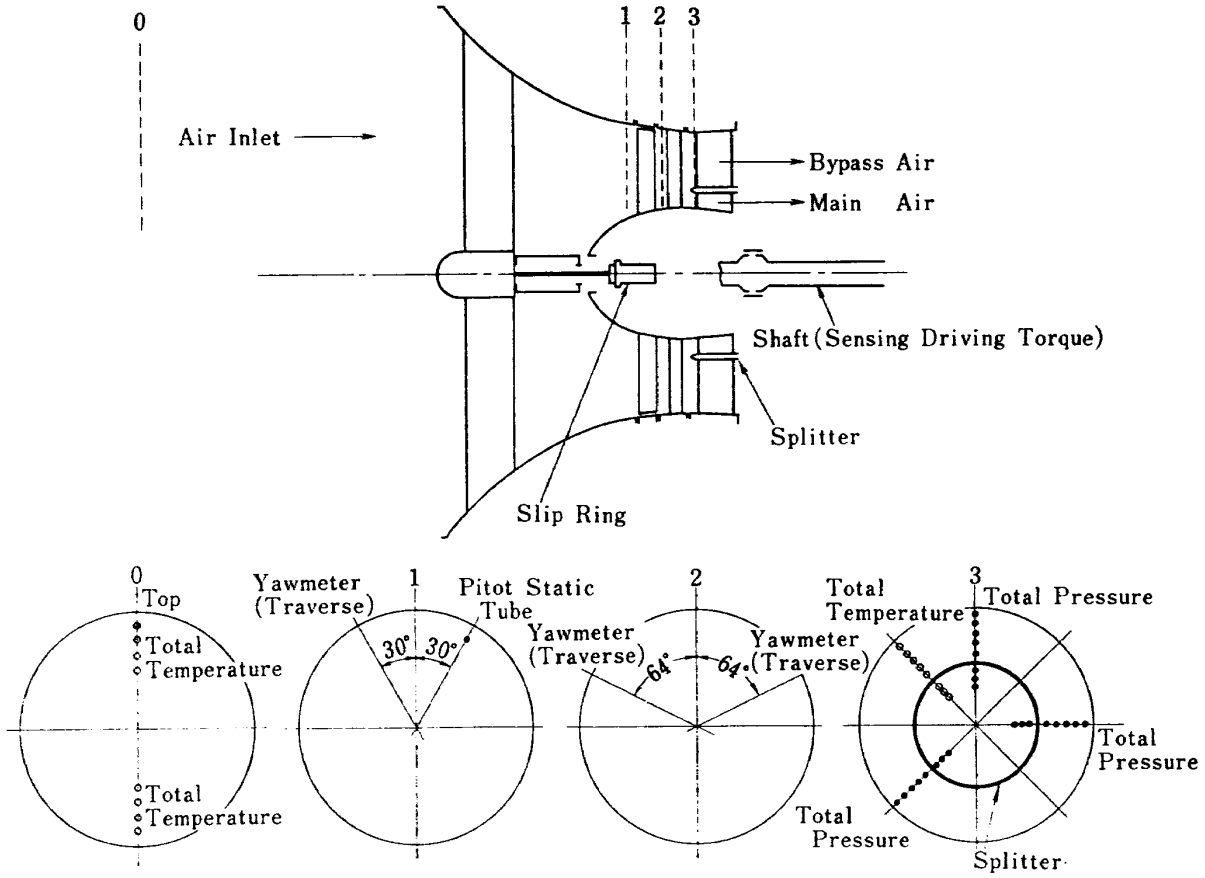

Fig. 6 Radial survey positions

height were assumed to be obtainable from using the read of another Pitot-static tube fixed at 61 millimeters from the outer wall, together with correlation curves based on the previously traversed data.

In the case of the three-hole yaw probe, the following quantity was defined to obtain the static pressure

$$\overline{H}=\frac{P_l+P_r}{P_0} \qquad (14)$$

where P_0 is the total pressure recorded by the probe center hole in balancing the left and right side hole pressure P_L, P_r, respecitively, and $\overline{H}$ is a function of Mach number alone if P_L is equal to Pr. Thus the Pitot tube was calibrated carefully in a wind tunnel to get a relation of $\overline{H}$ and Mach number. In testing the fan, $\overline{H}$ was easily obtained from the Pitot tube readings and, in combination with total pressure P_0 measurement, gave the static pressure value at the point in question.

At section '2' located in approximately 20 mm downstream the rotor, the flow direction, total and static pressures were traversed in some detail by the same procedure taken in the inlet section '1', with special reference to the flow leaving from the rotating blades at high rotational speeds.

In determination of total pressure and temperature after the stator blade row, four of eight struts at section '3' were utilized for mounting the probes; one strut used for the thermocouple probes and three struts for total pressure holes. The circumferential position of these three struts relative to the stator blade was selected by taking account of the predicted flow variation occurring in one stator pitch. It was assumed that a linear interpolation between two static pressure-tap readings at both outer and inner walls gave the static pressure distribution along the blade span at section '3'.

All thermocouples including those used for measuring the mass flow at the orifices were calibrated in a constant temperature oil of a portable bath tub, maintaining that relative position of thermometer probes and their connecting lines was the same in calibration as in testing the fan. Furthermore, to assist the measurement accuracy concerning the overall adiabatic efficiency, a driving torque was measured through the angle of twist produced in a predetermined length of the torsional shaft coupling the test vehicle with the driv-

ing shaft of the gasturbine. It was confirmed in the calibration that the torquemeter used here had a capacity of measuring range up to 500 kg-m and of maximum rotating speed 9000 rpm.

The rotative speed of the fan was counted on a digital meter making use of the pulse signal generated at a running gear in a magnetic field of a small box which was mounted on the rotating shaft of the gasturbine. During the operation of the fan, the monitor of stress level of a vibrating blade was successfully made by the output which strain gauges on the airfoil surface produced through a slip ring with maximum allowable alternating stress of 40 kg/mm² at the blade root.

EXPERIMENTAL RESULTS

Over-all performance

The performance map is indicated in Fig. 7 where the over-all weight flow means the summation of the bypass and main flows measured at the orifices. The characteristics of total pressure ratio and adiabatic efficiency versus mass flow are shown with rotative

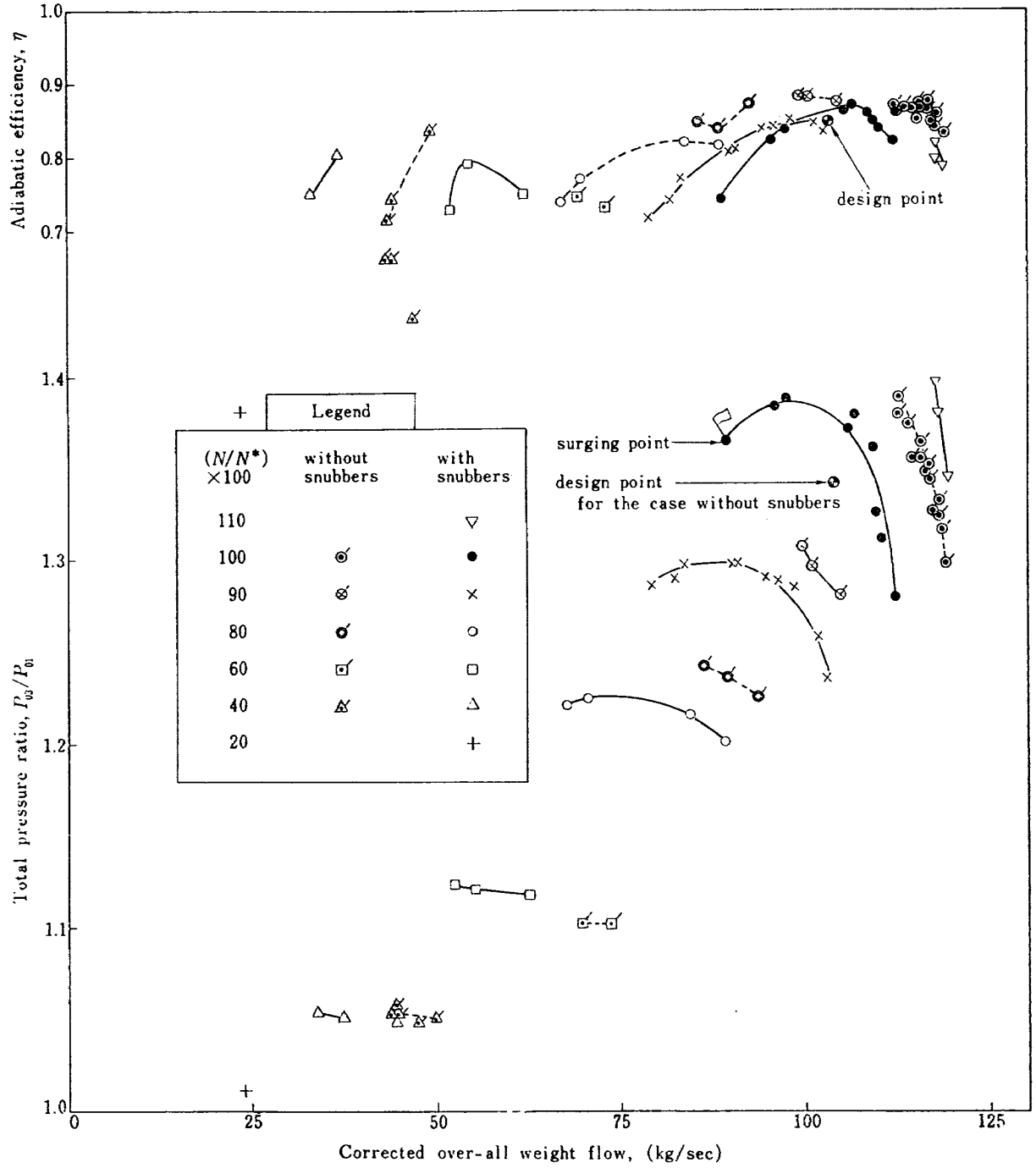

Fig. 7 Over-all aerodynamic performance

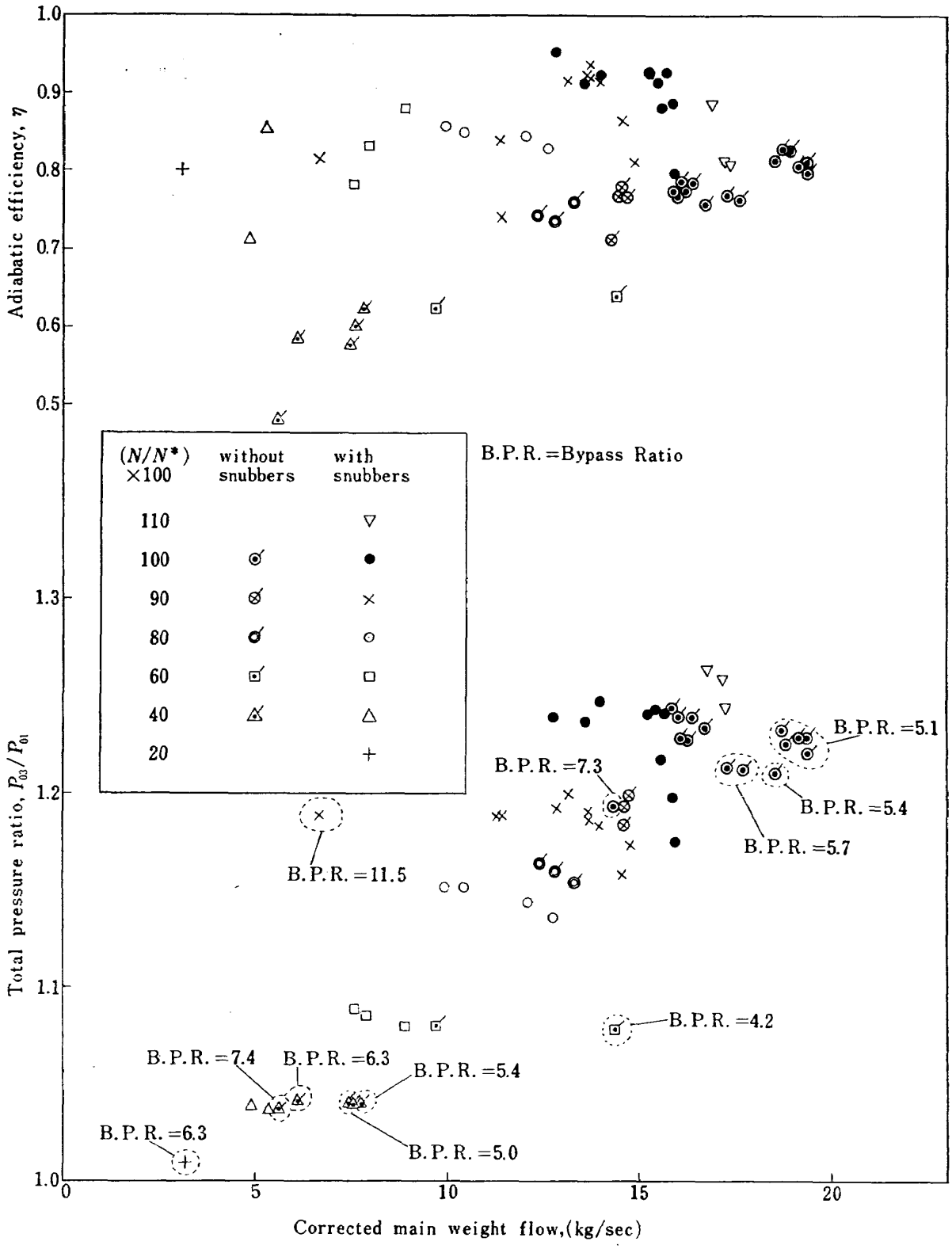

Fig. 8 Main-flow characteristics

speed ratio N/N* as a parameter; the data measured within a fluctuation of 0.5 per cent in the assigned rotative speed ratio were plotted. All data except for several points belong to the operating condition of the bypass ratio ranging from 5.90 to 6.10. The total pressure was defined as a ratio of the arithmetical mean value over 24 measured total pressure at the exit struts to the inlet total pressure just in front of rotor blade row. Generally the adiabatic efficiency was based on the evaluation of using the temperature and pressure data, and was subjected to some correction and adjustment which could be made

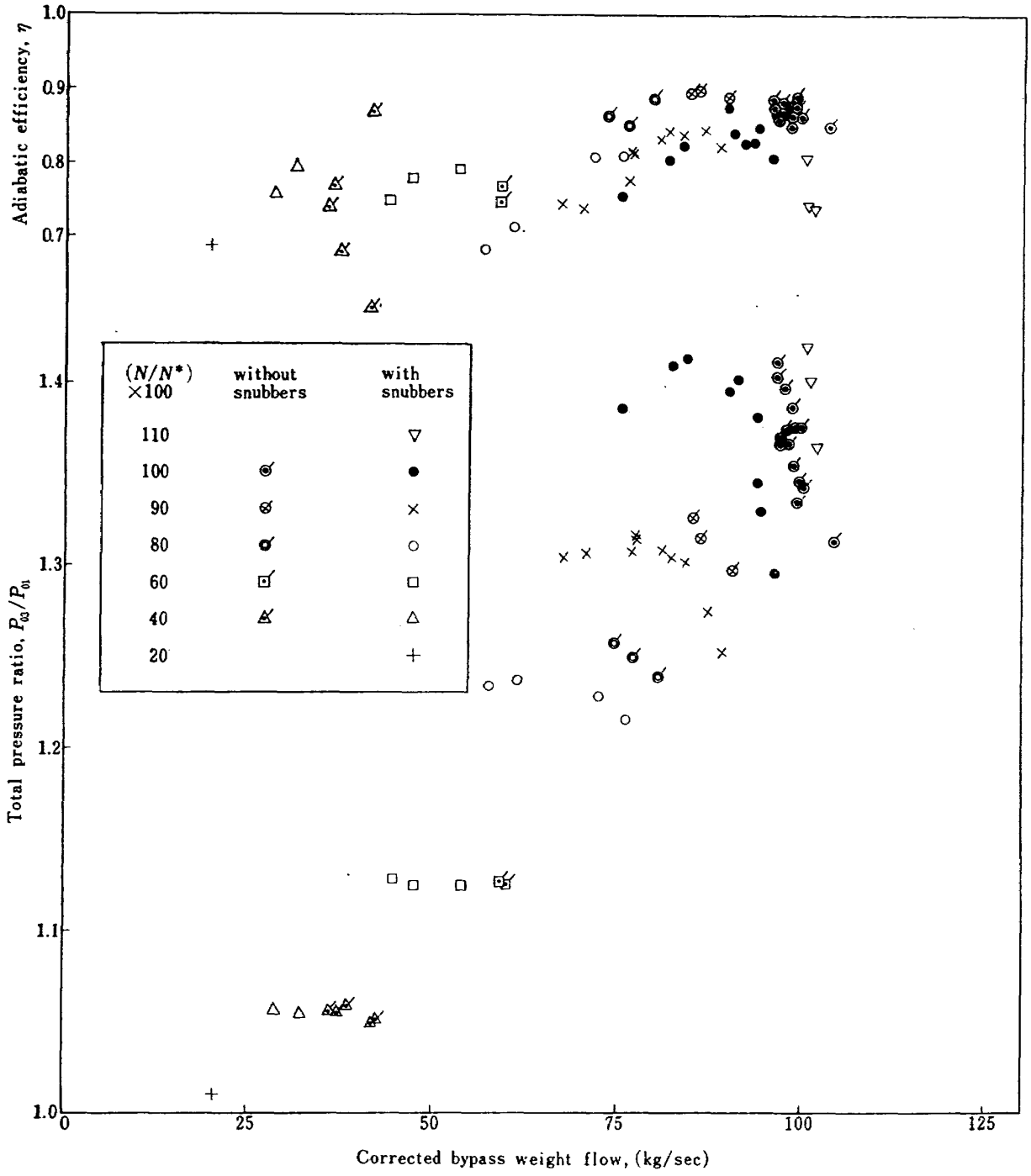

Fig. 9 Bypass-flow characteristics

with the aid of the torque measurement. The experimental data for the case without snubbers were limited; any data were not shown in the region near surge line because no operation of the fan was made in fear of the blade damage due to stall. On the other hand, in the case with snubbers, complete data for one surging point could be obtained at the designed rotative speed ratio with very small risk of damaging blades. However, further tracing of surge points at other rotational speeds was abandoned in order to avoid the repeating risk.

Comparing two cases with and without snubbers, the effect of them on the aerodynamic characteristics was clarified in terms of adiabatic efficiency, mass flow rate and total pressure ratio. For instance, there occurred approximately 7 per cent decrease of mass flow rate and an efficiency drop of almost 2.5 per cent at the designed rotational speed. Furthermore, also with snubbered blades, an overspeed operation exhibited another drop of efficiency. It is of interest to note that, for both cases, the measured data of pressure ratio versus mass flow showed considerably

higher values in comparison with the design point estimated for the no snubbered fan. The main source of this discrepancy will be discussed in the next internal flow section. No appreciable effect of snubbers could be seen on the overall performance map for lower rotational speeds, along with inherent inaccuracies in the adiabatic efficiency measurement.

To clarify the effect of the variation of a ratio of bypass to main flow on the performance characteristics, the over-all map was split into two diagrams of Figs. 8 and 9 representing each performance of the bypass and main flow sides. The operating point having the bypass ratio of well below and above the value of 6.0 was circled to indicate the bypass ratio (denoted as B.P.R.) in Fig. 8. The characteristic curve for the main flow was more influenced by the variation of bypass ratios than that for the bypass flow because the amount of main flow had a small share in the gross weight. The fact that the adiabatic efficiency for the main flow was lower in the no snubber case, contrary to our expectation, would be of most interest and hence will be discussed later in the next section from the internal-flow point of view.

Internal flow analyses

The flow behavior between blade rows and blade local performance thereby were obtained from the detailed survey data. The concept of streamline approach still remained in the data process to indicate the blade local characteristics more accurately in the flow region where a large amount of streamline displacements was observed. In other words, the blade element performance as a well-known technical term appeared to be of questionable expression because the usual treatment of blade element would be based on the assumption that a given streamline across a blade row be constant during any operation of a turbomachine. For example, Figs. 10 (a), (b) and (c) show the measured streamline distributions obtained from the survey data at each section, in the form of local weight flows divided by gross weight flow, where a comparison of the designed and uniform flow distributions also was made. The disturbance action of the snubbers reflected in upward radial flows at blade sections above them, Fig. 10 (b) and extended in almost whole blade span as the upward radial displacement of streamlines behind the stator blades, Fig.

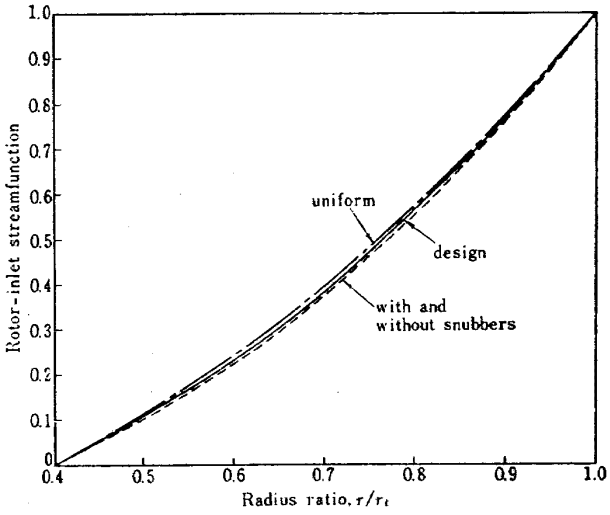

(a)

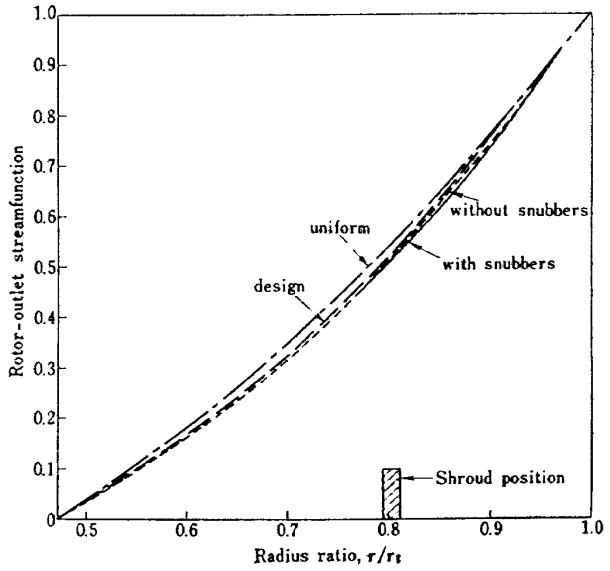

(b)

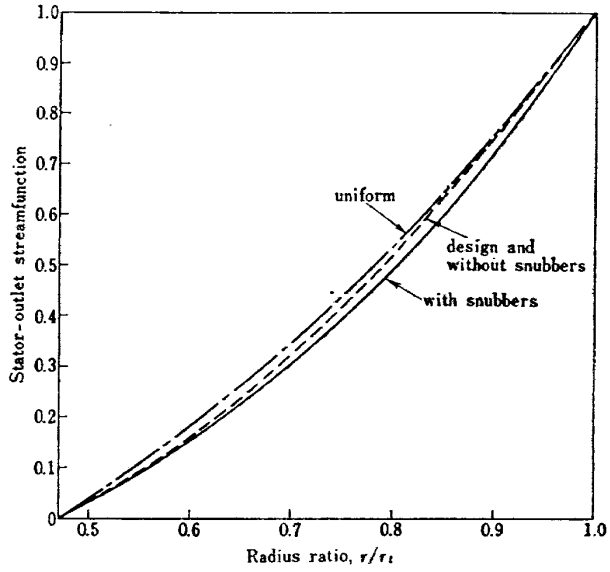

(c)

Fig. 10 Distribution of stream functions along hub-to-tip ratio

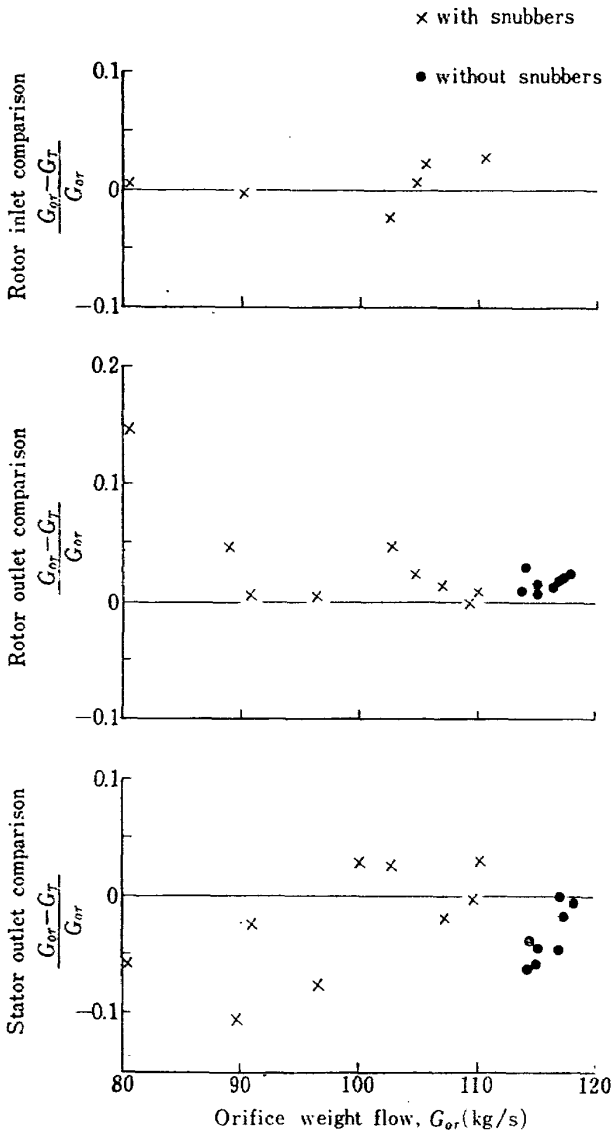

Fig. 11 Comparison of integrated and orifice flows

10 (c). Although not presented in a diagram, another streamline displacement due to the change of, say, incidence angles was also observed.

To determine the internal flow behavior the traversing data were gathered at approximately 10 points of high-speed operation of the test vehicle for both cases respectively. As one of the methods for evaluating the reliability of the measured data, comparisons of the integrated weight flows at the blade inlet, outlet measuring stations with the values measured at the orifices are presented in Fig. 11. The majority of the integrated flows at each section was well within ±5 per cent of the orifice measured flows. Since no detailed traversing was made in front of the rotor blades without snubbers to eliminate the risk attending a dangerous contact of vibrating blades with the yaw probe, the correction curve was used to determine the inlet flow condition, as stated in the chapter of the instrumentation.

In traversing the snubbered rotor outlet section '2', approximately 17 points along the blade height were selected as the position to be measured; traversed at 2.0 mm intervals for the wake influenced region due to the snubbers; at almost 20 mm intervals for the other. While, in the flow field after the rotor without snubbers, the yaw probe was usually read at 5 points having about 40 mm intervals along the blade span.

The survey raw data about the total pressure, flow angle and absolute resultant Mach

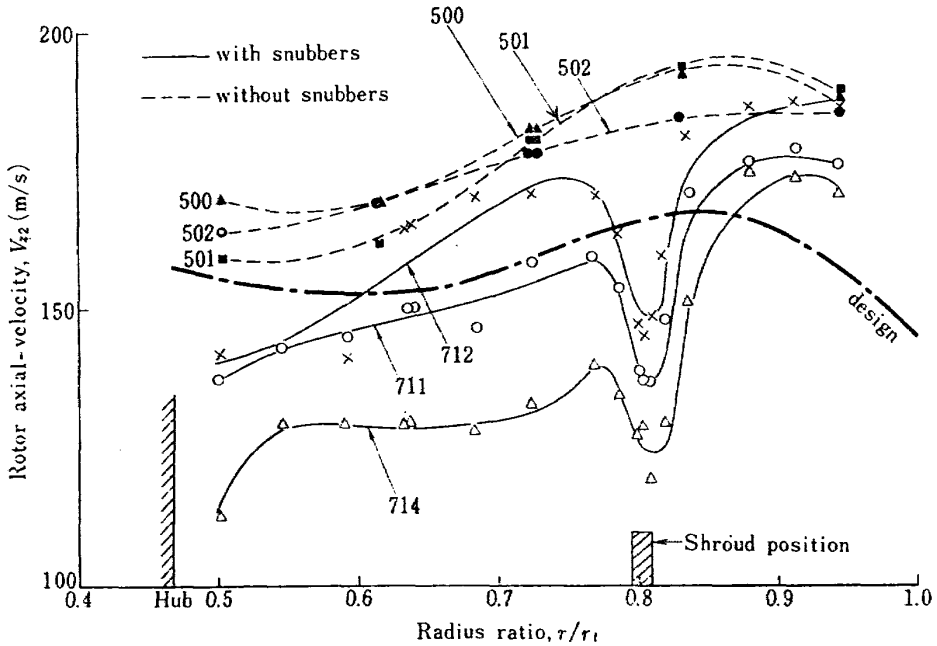

Fig. 12 Axial-velocity distribution

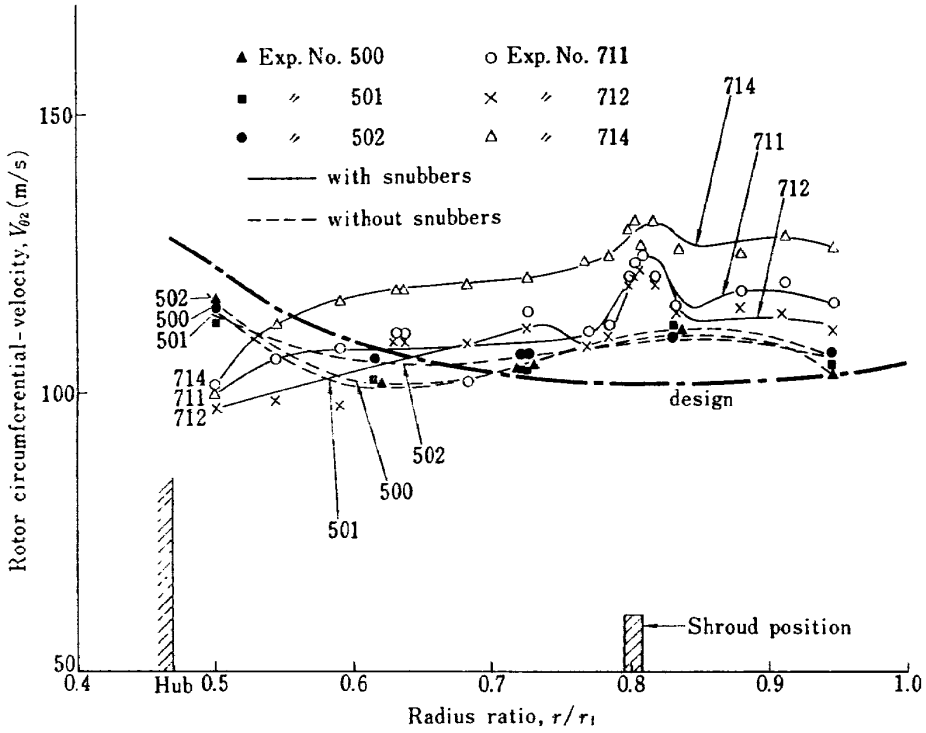

Fig. 13 Circumferential velocity distibution

Table 2 Experiment numbers chosen to illustrate the radial distribution of the survey date

Experiment No.		Over-all weight flow (kg/s)	Pressure ratio	Rotative speed ratio (%)	Bypass ratio
without snubbers	500	117.8	1.350	101.3	6.312
	501	116.0	1.354	100.4	6.188
	502	114.9	1.353	99.3	6.103
with snubbers	711	106.9	1.377	100.6	5.915
	712	109.5	1.359	100.4	5.991
	714	96.6	1.384	98.7	5.882

number were, interpolated by use of the least-mean-squares curves with 3rd or 4th order or combination of 3rd and 4th order depending on the situation. Therefore, both the interpolated curve and survey data themselves were utilized to reduce the measured data for obtaining the flow behavior and local blade characteristics

To some extent, each component of the measured velocity will reflect the flow movement between blade rows. Thus, typical three cases of test data and their interpolated least-mean-squares curves respectively for the both fans were chosen to show the radial variation of axial and tangential velocities at the rotor outlet in Figs. 12 and 13. The explanation of the designate experiment numbers is given in the Table 2. The distribution of the measured and prescribed velocities was very similar for no snubber case. On the contrary, the disturbance caused in a velocity field was not confined to a small portion influenced by wakes shedding from snubbers, but extended over the whole blade span. Especially the peak value of tangential velocity of Fig. 13 appeared at the radial position corresponding to the upper surface of snubbers and towards hub section the tangential velocity remarkably decreased. The rotor blade turning angle distributions shown in Fig. 14 indicate that the presence of snubbers disturbed the turning angles even in the hub region. Note that in presenting the angle the survey data themselves could not be plotted because they had

no definite meaning in a flow field attended with unpredictable streamline displacement. The rotor turning angles as it is generally defined will fully depend on the relative angles before and behind the blade row, and hence on the streamline displacement across the blades. Then the least-mean-squares curve representative of turning angles was obtained by a subtraction of inlet and outlet relative angles placed on the same streamline across the blade row, making use of the corresponding interpolated curves.

The relationship of deviation, incidence angles and relative Mach number at three radial positions is presented in Figs. 15 and 16. The deviation and incidence angles were based on the calculation of using the inlet, outlet angles measured and the blade angle tangent to the mean camber-line of airfoil at the leading and trailing edges. In addition, the correction of axial velocity ratio across the blade row was made in the deviation angles by the relation $(\delta-\delta_{\text{des.}})_{\text{corr}}=-K(VR-VR_{\text{des.}})$, where VR is the ratio of inlet to oulet measured axial-velocity and the value of constant K was selected as 10 degrees according to the experimental result of Pollard and Gostelow [8]. The values thus corrected are the deviation angles that would be realized if the flow passed the rotor blade row in the designed axial-velocity ratio, $VR_{\text{des.}}$ As indicated in Fig. 15 the measured deviation angles at the near root section was higher in 2~4 degrees than the designed value within the scattering range of data points for no snubber case. At other sections, however, 3~4 degrees turned out to be lower than the estimation. Even in the snubbered case almost the same trend was seen at all radii except for the near hub section where 6~10 degrees in the deviation angle was higher than expected. Then it was again shown experimentally that snubbers of mid-span had a remarked influence on the deviation angles in the hub regions. On the other hand, from a simple

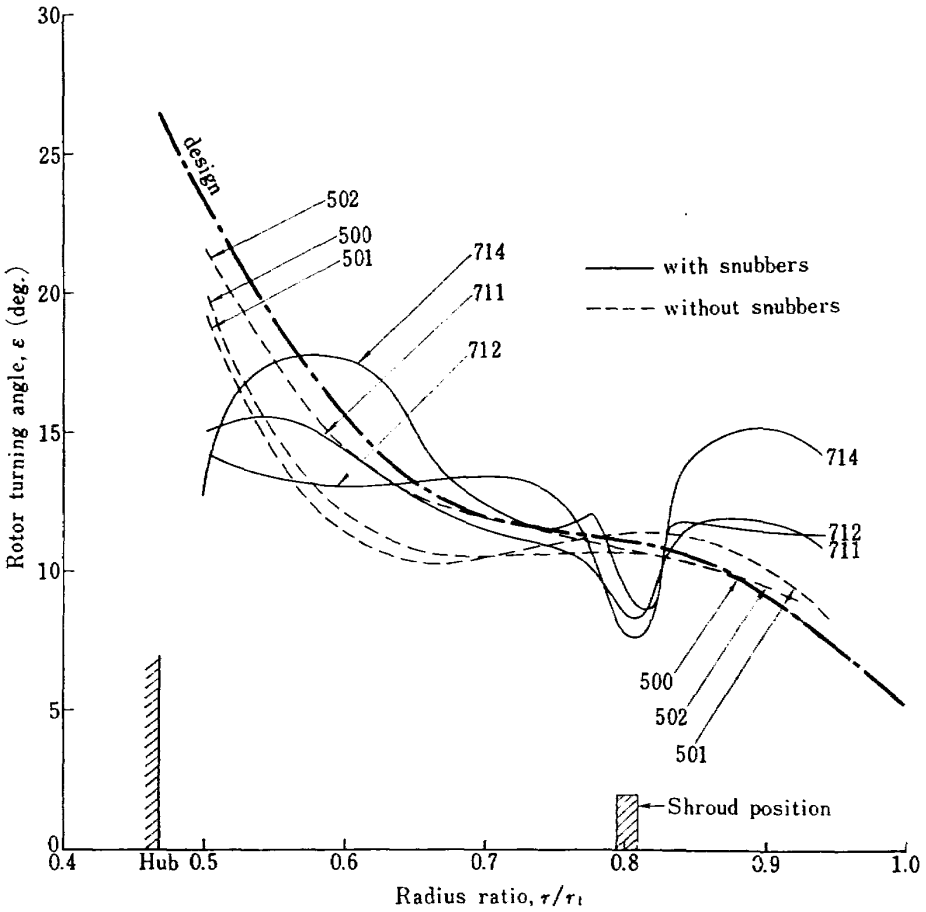

Fig. 14 Turning-angle distribution

computation it was concluded that the untwisted moment acted on the high staggered blade row due to the centrifugal force might be the main source for the low magnitude of deviation angles appeared at mean and tip sections. Apparently the higher values of mass flow and total pressure ratio indicated in the over-all performance map of Fig. 7 were produced by the lower deviation angles than expected, and at the same time it is fairly said that higher devaition angles in hub regions had a great part in the deterioration of aerodynamic characteristics curves of the snubbered fan.

The rotor loss-parameter defined as $(\theta/c)_r = \varpi \cos\beta_2'/2\sigma$ was plotted against the diffusion factor in Fig. 17. Similar to the procedure taken for presenting the turning angle diagram, the data reduction of loss-parameter was based on the use of two interpolated curves across the blade row to incorporate the streamline displacement so that the total pressure loss occurring on the same streamline might be treated. Since the values of diffusion factor obtained in the radial survey were not so large, it was not easy to bring the loss parameter into proper correlation with the blade loading. Moreover, typical six experiment numbers were chosen again, corresponding to Fig. 14. to show the radial variation of loss parameter in Fig. 18. The relatively higher value of loss indicated in the experiment number 714 was due to higher incidence angles than the others, looking back to Fig. 16. The

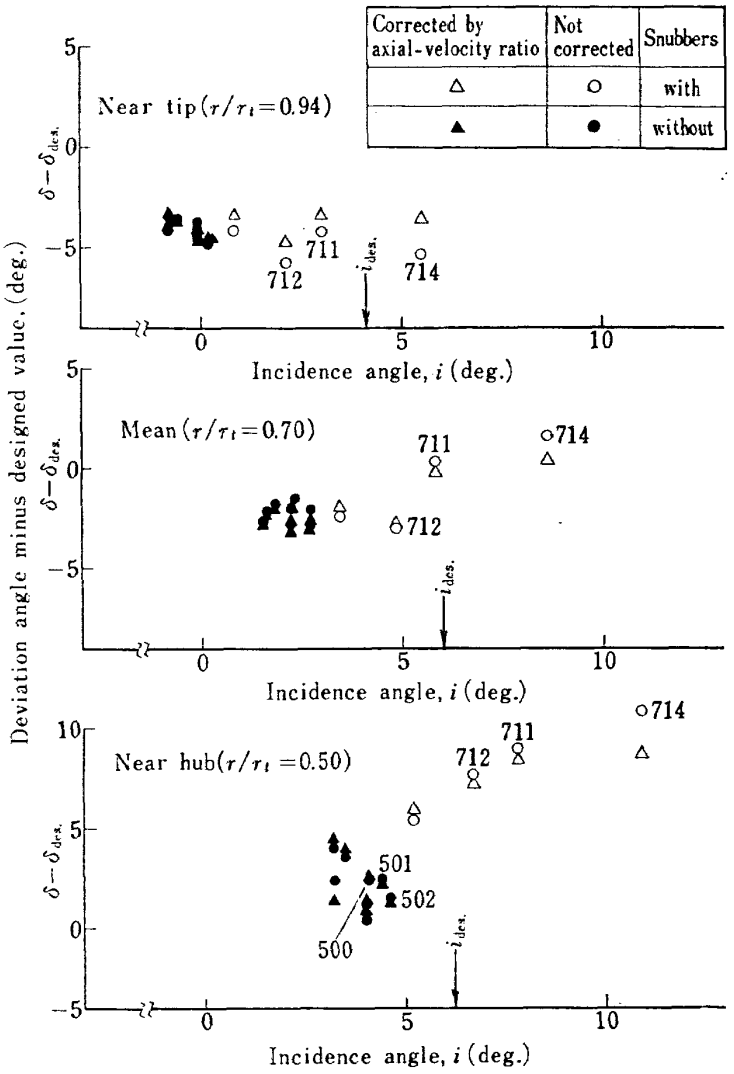

Fig. 15 Rotor deviation angles minus designed values against incidence angles at three radial sections

most striking feature is the low magnitude of loss measured in the hub region for the snubbered blades. It follows that the higher adiabatic efficiency of the main flow for the snubbered case would appear. The main reason for the decrease of loss-parameter may be attributed to the lower levels of relative Mach number as observed in the snubbered blade hub region, Fig. 16. In fact, from the authors' experience the rotor hub section of usual compressors in the aerodynamic performance has been very sensitive to the relative Mach number level to be operated.

The radial variation of total pressure is presented in Fig. 19. The similarity of no snubber case and design distribution was almost maintained, while the disturbance effect of snubbers was noticed even in the blade tip and hub regions as previously pointed out.

In the case of the fan without snubbers, a larger amount of weight flow than the designed value resulted in the lower incidence angles entering the stator blades along the whole blade height, as shown in Fig. 20. In the fan with snubbers, positive incidence angles amounted to 10~15 degrees in the region where a wake type of decreased axial-velocity profile existed. The loss-parameter across stator blades and entering Mach number distributions are presented in Figs. 21 and 22 respectively. Higher levels of loss-parameter of the stator behind the rotor without snubbers might be due largely to the lower incidence angles plus higher inlet Mach number

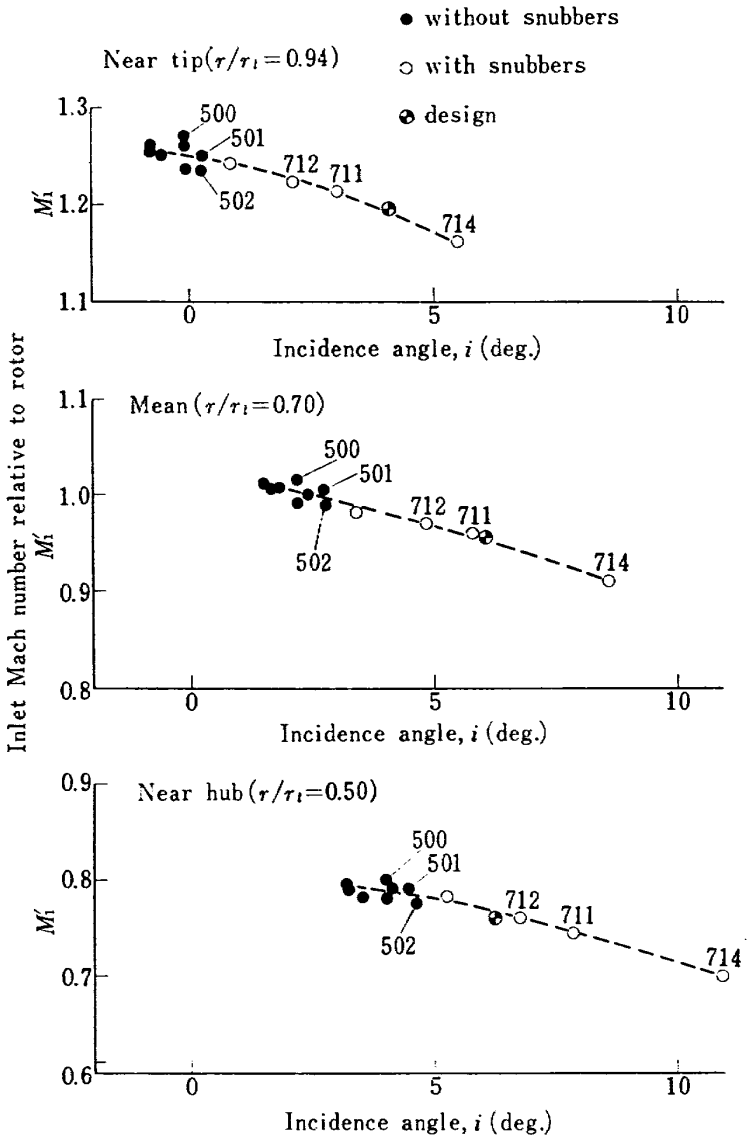

Fig. 16 Rotor inlet Mach number versus incidence angles

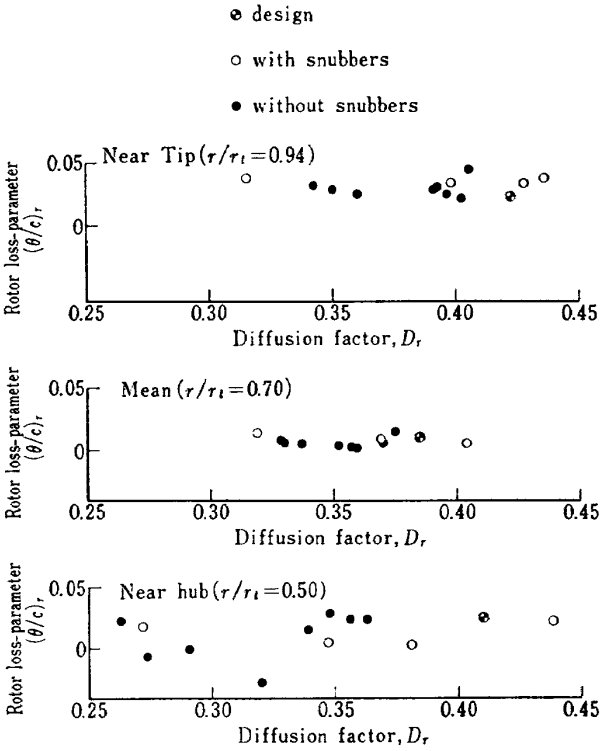

Fig. 17 Rotor loss-parameter against diffusion factor at three radial sections

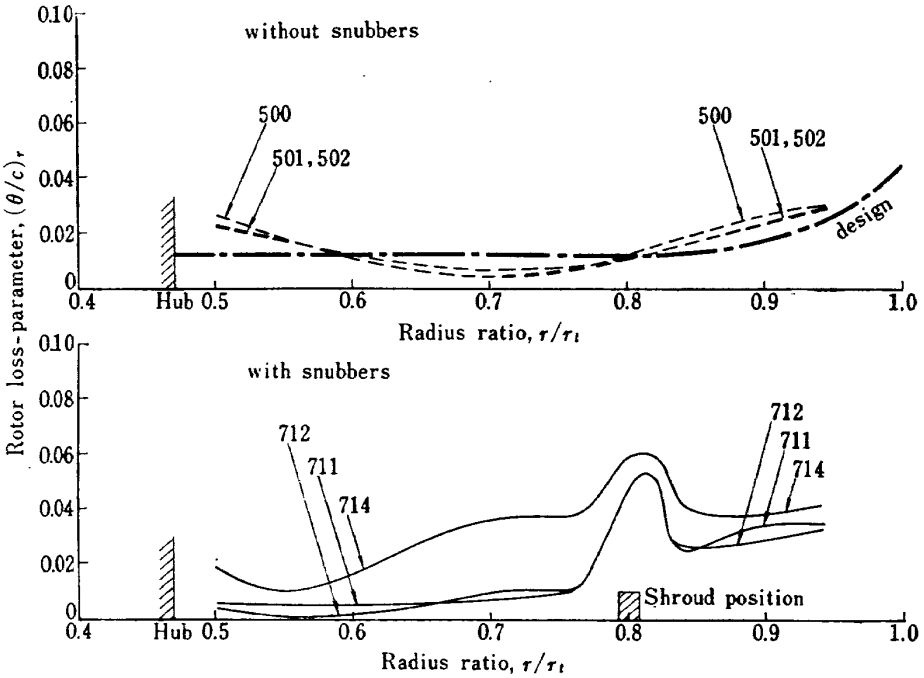

Fig. 18 Radial distribution of loss-parameter across rotor blade row

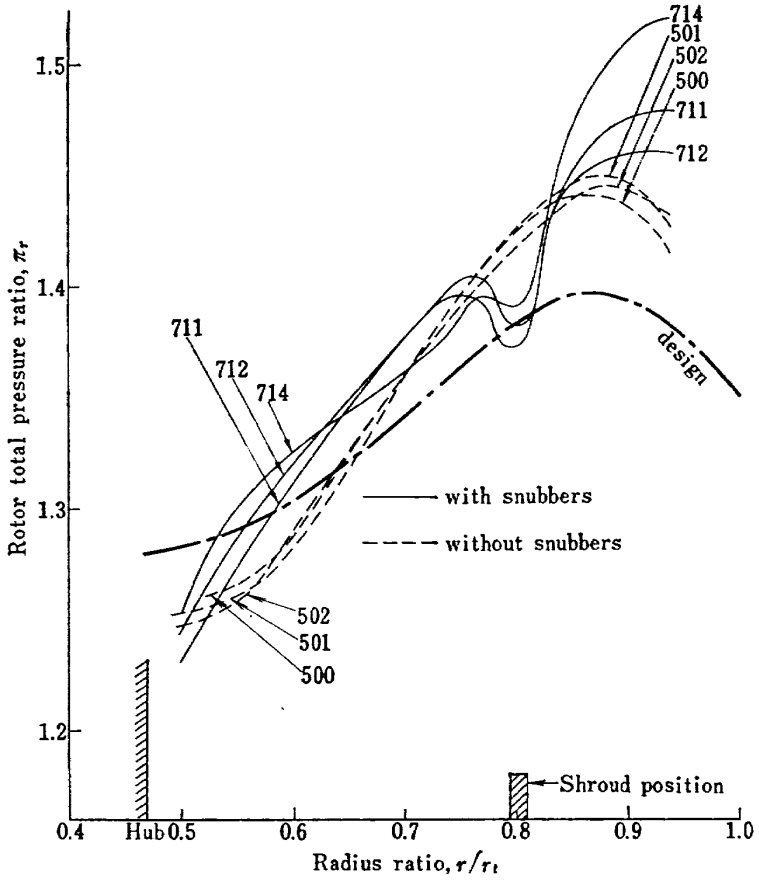

Fig. 19 Radial distribution of total pressure ratio across rotor blade row

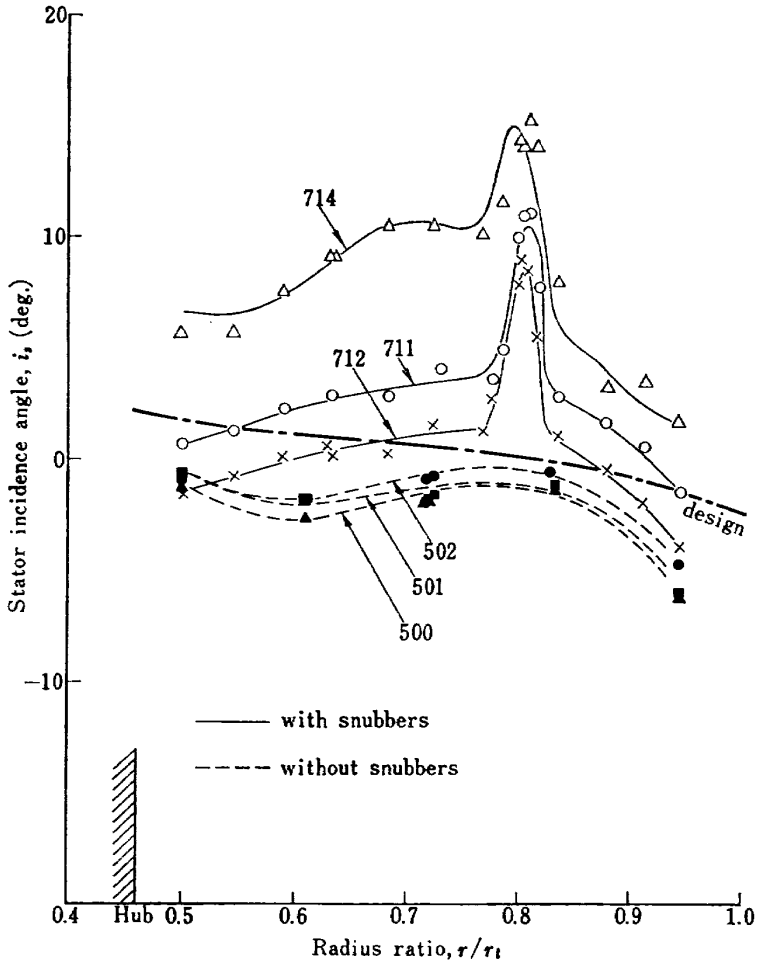

Fig. 20 Radial distribution of incidence angles entering stator blade row

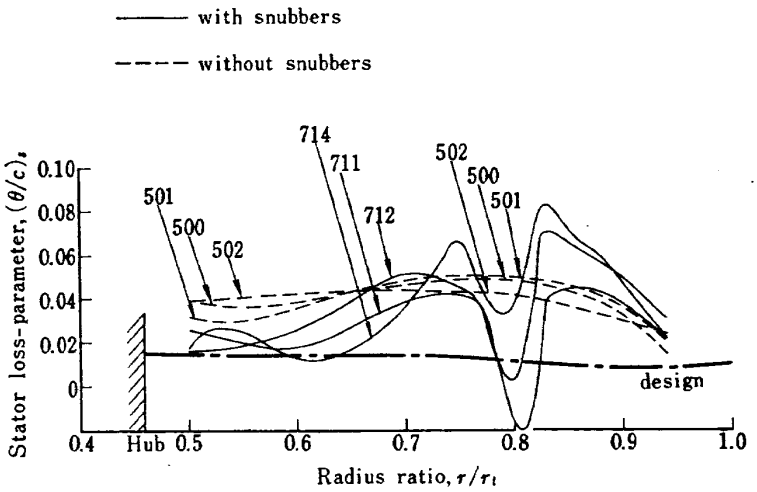

Fig. 21 Radial distribution of loss-parameter across stator blade row

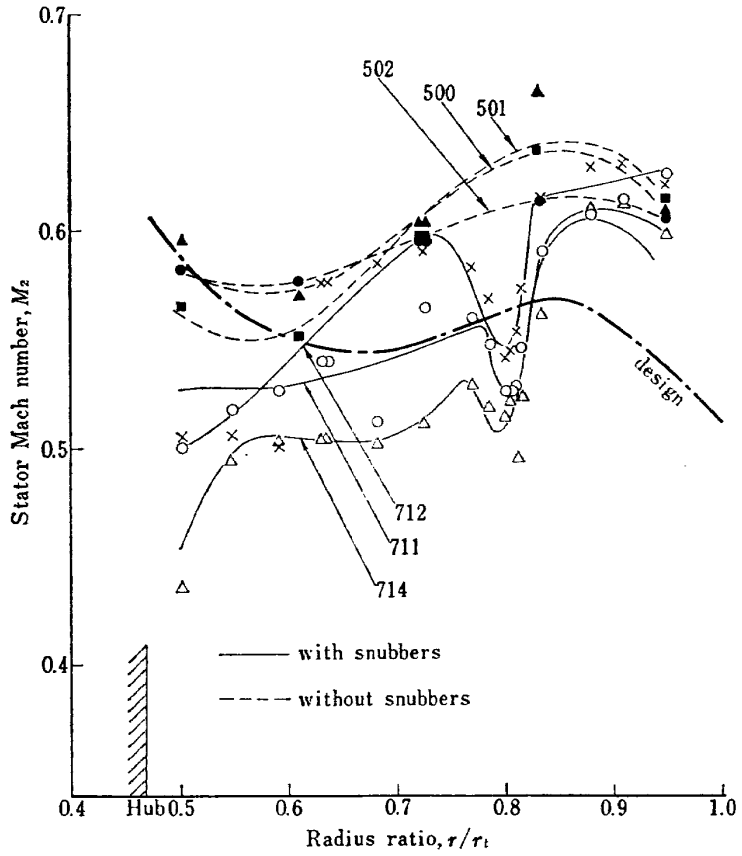

Fig. 22 Radial distribution of Mach number entering stator blade row

than the designed. While, lower levels of the stator hub loss-parameter for the fan with snubbers, contrary to our expectation, could be attributed to the lower entering Mach number due to the reduction of mass flow near the hub section. Extremely low levels of loss were observed in the middle of the blade sections influenced by the snubber wake, and maximum values of loss-parameter appeared in the regions outside the wake. As a result of some detailed check of raw data regarding the total pressure, it was evident that the spread of the wake in passing through the stator blades produced such a peculiar shape of loss-parameter. Also the appearance of negative value of loss-parameter might be interpreted as follows: eight radial survey probes situated at the exit strut were not enough, in some cases, to provide sufficient data for the wake influenced portion in the stator outlet region.

The radial variation of total pressure ratio across the rotor and stator blade rows is shown in Fig. 23. The lower pressure ratio appearing in the hub regions for both cases is indicative of the flow underturning across the rotor blades.

To determine the characteristics of the snubber wake behind the rotor blades, the displacement δ_z^* and mometum thickness θ_z in axial direction can be defined by the following equations

$$\int_0^{\delta_z^*} \rho U_p r dy = \int_0^{\delta} \rho (U_p - V_z) r dy \qquad (15)$$

$$\int_0^{\theta_z} \rho U_p^2 r dy = \int_0^{\delta} \rho V_z (U_p - V_z) r dy \qquad (16)$$

where δ is the radial distance covering the wake influenced portion at about 20 mm downstream of snubbers, the origin of y is the point at which the wake begins, U_p is the axial velocity that would be present with snubbers removed, and V_z is the measured axial velocity in the wake region. In actual computation, referring to Fig. 12, all measured data except for the wake influenced data points were fitted by the 4th order least-mean-squares curve which was assumed to be the analytical expression of U_p and ρU_p. On the other hand, the 3rd order least-mean-squares curve was used for fitting the data

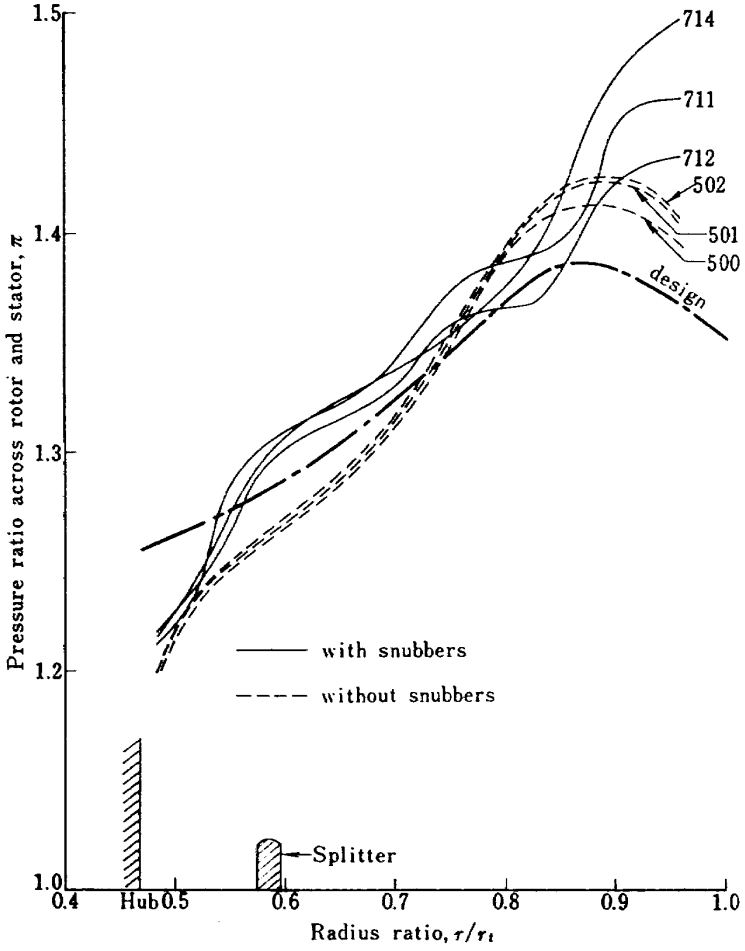

Fig. 22 Radiaisl distribution of total pressure ratio across the fan stage

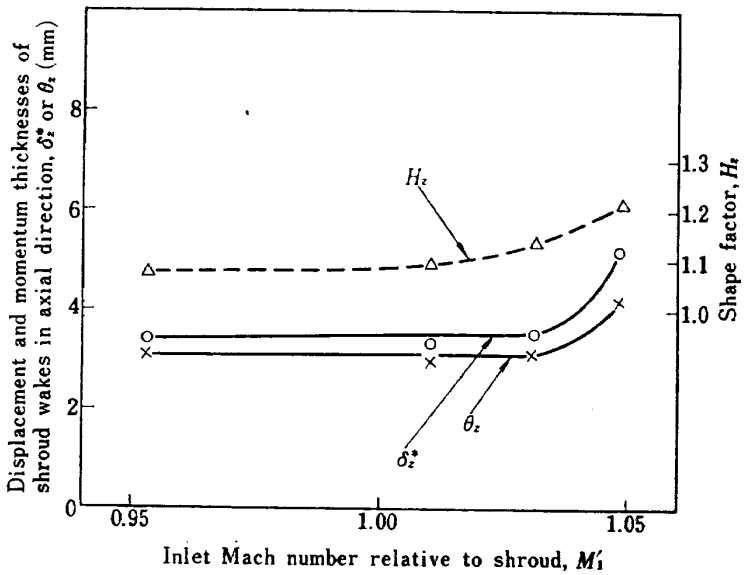

Fig. 24 Characteristics of the wakes shedding from the shroud against inlet Mach number

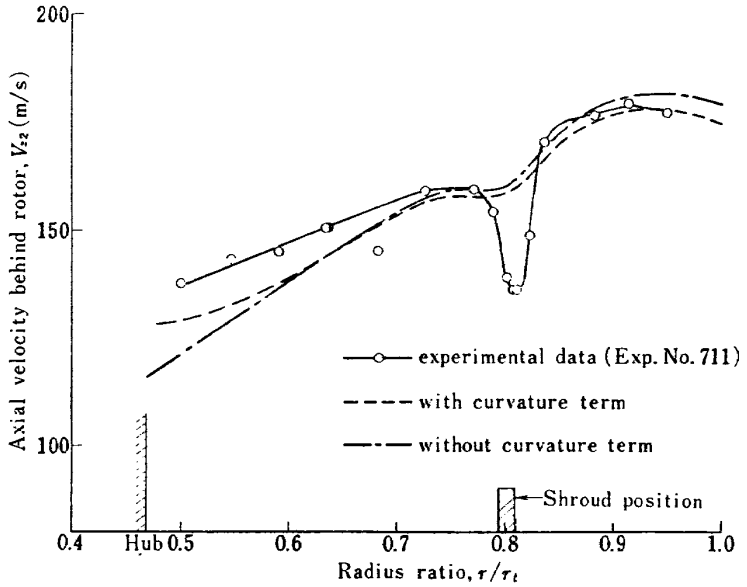

Fig. 25 Comparison of measured and computated axial-velocity distribution

points in the snubber wake region in order to make curves of V_z and ρV_z. Hence δ_z^* and θ_z were obtained in solving sixth and tenth order algebraic equations regarding the values of δ_z^* and θ_z respectively, according to the equations (15) and (16). The results are shown in Fig. 24. The wake properties of δ_z^*, θ_z appeared with consistent variation according as the increase of entering resultant Mach number relative to snubbers. It is clearly seen that the wake of snubbers having blunt leading edges increasingly deepened and widened in the inlet Mach number beyond 1.03, this value having been equivalent to an axial component of 0.66 if the swept angle of snubbers was taken into consideration.

Last of all, the radial-equilibrium equation (6) was again solved in insertion with the measured data themselves of the tangential velocity, total pressure and temperature at each survey station. An example of these calculation results is presented in Fig. 25, indicating a questionable validity of the radial-equilibrium equation neglecting the local shearing stress in the strong viscous region behind snubbers, even with the inclusion of streamline curvature, cumulative losses and total temperature gradient as accurately as possible. A result of computation with the streamline-curvature term alone suppressed was also added so that the effect of streamline movement on the axial velocity profile might

be examined. It is then hoped that this illustration would make a contribution toward the promotion of the establishment of the viscous flow analysis, for which further work is needed in the axial-flow turbomachinery [10].

CONCLUSION

The component research of the front fans had been conducted to advance the aerodynamic design, experimental technique as well as manufacturing technology. Among them this paper treated mainly the aerodynamic aspect of the fans.

In connection with design work, a computation technique with the streamline-curvature term included was studied in some detail, with the result that the least-mean-squares curve of sixth order was most suitable for defining each streamline in 9~15 stations. Thus, the computing procedure was effectively used for evaluating the internal flow field, where a steep radial variation of temperature and pressure was inevitable at the design condition. Furthermore, the detailed analyses of survey test data for the internal flow were also made using the streamline displacement concept.

The research program fairly progressed in two steps; first, the fan without snubbers was partially investigated and next, the experiment of the snubbered fan was carried out to determine the effect of snubbers on the aerodynamic characteristics. As a result, the over-all performance for both cases turned out to be better than expected; over-turning of the rotor blade mean and tip sections produced higher values of total pressure ratio and weight flow. The main source for low levels of the rotor deviation angles in the mean and tip regions was the untwist of the rotor blades due to the centrifugal force. Therefore, the deviation angles indicated should be considered as the apparent values, which will need some correction in the future. Nevertheless, it was confirmed experimentally that the front fan with snubbers could gain a pressure ratio of 1.38, weight flow rate 100 kg/s and adiabatic efficiency of 84 per cent at a rotor tip peripheral speed of 380 m/s.

A thorough comparison of the radial survey data revealed that the disturbance due to the presence of the snubbers was not only confined to the narrow portion of the snubber wake, but extended over the other sections of the rotor blades. It may be said that since the flow between blade rows is being governed by a combination of radial equilibrium and continuity equations, a local disturbance produced at the part span will upset the radial balance designed for no snubber fan, and a new equilibrium will be established in the spoiled flow field. In fact, the aerodynamic performance of rotor hub section was severely influenced by snubbers.

There are still left some studies of determining aerodynamic performance and snubber retaining-effectiveness in a flow field subjected to various inlet distortions. Furthermore, the development of more powerful means for abating fan noise would be sincerely hoped.

To boost the lower pressure ratio in the hub region of the fan, a study of small multi-stage compressor rotating simultaneously with the front fan shaft is now in progress aiming at practical application to a fanned jet-engine.

ACKNOWLEDGEMENTS

This study was conducted under the supervision of Dr. M. Matsuki, Head of Aero-Engines Division, National Aerospace Laboratory, with cooperation many other colleagues. Especially the authors wish to thank Mr. T. Torisaki, Engine Performance Section Chief, for his valuable advice. The test vehicle was manufactured by the Ishikawajima-Harima Heavy Industries, Tokyo.

REFERENCES

[1] Wu, C. H. and Wolfstein, L.: 'Application of Radial-Equilibrium Condition to Axial-Flow Compressor and Turbine Design', NACA Rep. 955, 1950.

[2] Von Brammert and Fiedler, K.: 'Strömung in axialen Turbomaschinen', Ingenieur-Archiv, 33, pp. 322~329, 1964.

[3] Novak, R. A.: 'Streamline Curvature Computing Procedures for Fluid-Flow Problems', ASME Paper No. 66-WA/GT-3, 1966.

[4] Walsh, J. L., Ahlberg, J. H. and Nilson, E. N.: 'Best Approximation Properties of the Spline Fit', Journ. of Math. and Mech., Vol. 11, No. 2, pp. 225~234, 1962.

[5] Fujii, S. and Uno, T.: 'Streamline-Curvature Approach to Duct-Flow Problems', National Aerospace Lab. Technical Report TR-140, 1967.

[6] Fujii, S. and others: 'The Aerodynamic Performance of a Single-Stage Axial-Flow Compressor with Double-Circular-

Arc Blades', National Aerospace Lab. Technical Report TR-134, 1967.

[7] Fujii, S., Matsuki, M. and Gomi, M.: 'The Five-Stage Transonic Compressor for Lift Engines—Aerodynamic Design—', National Aerospace Lab. Technical Memorandum TM-114, 1967.

[8] Pollard, D. and Gostelow, J. P.: 'Some Experiments at Low Speed on Compressor Cascades', Trans. of the ASME, Series A, 89, pp. 427~436, 1967.

[9] Levine, P.: 'Incompressible Potential Flow about Axially Symmetric Bodies in Ducts', Journ. of Aerospace Sciences, pp 33~36, 1958.

[10] Fujii, S. and others: 'Some Observations on the Velocity Profiles in Fully Developed Viscous Flow in Turbomachines', ASME Paper 70-WA/FE-24, 1970.

APPENDIX (A)

The stream function ψ for the incompressible, axi-symmetric flow may satisfy the equation

$$\frac{\partial^2\psi}{\partial z^2}+\frac{\partial^2\psi}{\partial r^2}-\frac{1}{r}\frac{\partial\psi}{\partial r}=0 \qquad \text{(A-1)}$$

The incompressible flow around a point source of the strength m_0 at $z=r=0$, plus a uniform velocity U in an infinitely long duct of constant diameter was expressed by Levine [9] in the following form,

$$\frac{\psi}{U}=-\frac{m_0}{U}\nu^2-2\frac{m_0}{U}\nu\sum_{n=1}^{\infty}\frac{e^{j_nZ}}{j_n\cdot J_0^2(j_n)}\times J_1(j_n\nu)+\frac{\nu^2}{2}, \qquad (Z<0) \quad \text{(A-2)}$$

$$\frac{\psi}{U}=\frac{m_0}{U}\nu^2+2\frac{m_0}{U}\nu\sum_{n=1}^{\infty}\frac{e^{-j_nZ}}{j_n\cdot J_0^2(j_n)}\times J_1(j_n\nu)+\frac{\nu^2}{2}-2\frac{m_0}{U}, \qquad (Z>0) \quad \text{(A-3)}$$

where $\nu=r/r_t$, $Z=z/r_t$ and J_n means the first kind Bessel function of n th order, and j_n is the root of $J_1(j_n)=0$ $(n=1, 2, \cdots)$. In the case of $m_0/U=0.2$ the streamline movement is visualized in Fig. (A-1).

On the other hand, the same flow corresponding to $m_0/U=0.2$ was solved by making use of streamline curvature technique in which the streamline $\psi=0$ could be replaced by a wall boundary. In this case the radial equilibrium equation (6) reduced to,

$$V_z^2=c_1^2e^{\int\frac{2}{r_c\cdot\cos^2\lambda}dr} \qquad \text{(A-4)}$$

Then, as indicated in Fig. (A-1), 9 sections were placed in axial direction and the least-mean-squares curve of 6th order was used to define the streamline.

The computational result revealed that the agreement of both exact solution and streamline-curvature velocity-profile was fairly good

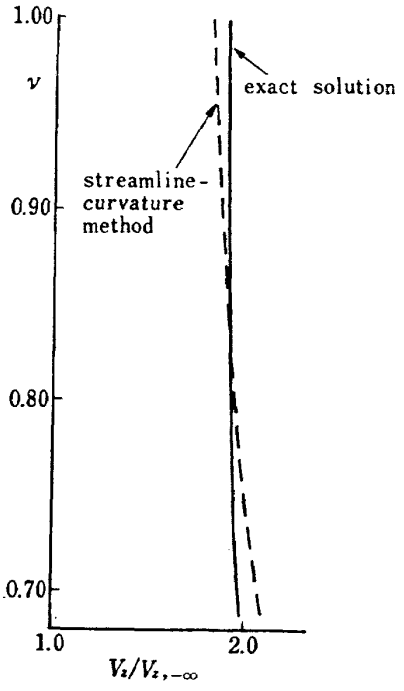

Fig. A-2 Comparison of axial-velocity calculated using streamline curvature method and exact solution at section ⑦.

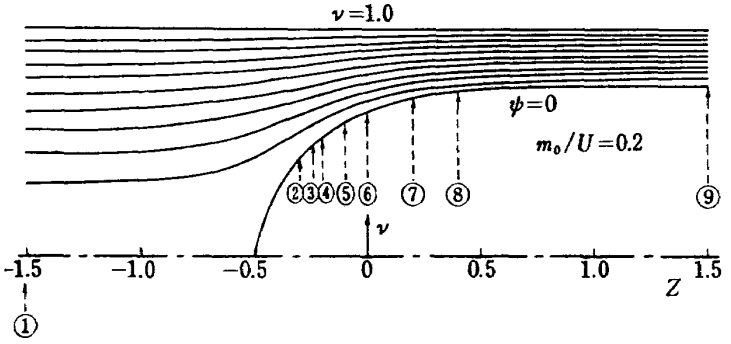

Fig. A-1 Streamlines obtained from exact solution

at sections 7 and 8, are Fig. (A-2). Nevertheless, the remarked difference between both profiles was seen at sections 2 and 3 where the effect of stagnation or singular point might appear strongly. It then led to a tentative conclusion that the streamline curvature computing procedure might have capability of giving a reliable solution for the flow in the region not close to a stagnation point or in a boundary wall without extremely small radius of curvature.

TR-258	Three Dimensional Suboptimal Explicit Guidance for Space Vehicles	Koji OTSUBO	Jan. 1972
TR-259	Study on a Rotary-Drive, Vibratory-Output Rate Gyro	Hiroshi YAMADA	Jan. 1972
TR-260	A High Sensitive Total Atmospheric Temperature Measuring Apparatus	Kenji NISHIO, Hiroyuki NOSE, Takeshi KOSHINUMA, Shigeo INOUE, Hiroshi USUI & Toshimi OHATA	Jan. 1972
TR-261	Strain Measurement of Solid Propellant Materials with Birefringent Coating	Sinichi KOSHIDE	Jan. 1972
TR-262	A Structural Analysis of Cylinder-Cone-Cylinder Shells by F.E.M.	Akinori OGAWA	Jan. 1972
TR-263	A Study of Subsonic, Two-Dimensional Wall-Interference Effects in a Perforated Wind Tunnel with Particular Reference to the NAL 2m×2m Transonic Wind Tunnel	Masao EBIHARA	Jan. 1972
TR-264	Flight Control System Design for Launch Vehicles with Liquid Propellant	Hidehiko MORI, Hajime KOSHIISHI	Jan. 1972
TR-265	Fluidic Turbine Inlet Gas Temperature Sensor	Kenji NISHIO, Seiki ENDO & Tokukazu ENDO	Jan. 1972
TR-266	Some Considerations on the Aerodynamic Characteristics for a Body of Rocket with Blunt Nose	Iwao KAWAMOTO	Jan. 1972
TR-267	Aerodynamic Design and Test Results of Front Fans	Shoichi FUJII, Hideo NISHIWAKI, Mitsuo GOMI, Noboru SUGAWARA & Katsumi TAKEDA	Jan. 1972

TECHNICAL REPORT OF NATIONAL AEROSPACE LABORATORY
TR-268T

航空宇宙技術研究所報告 268T 号 (欧文)

昭和 47 年 1 月 発行

発行所 航空宇宙技術研究所
東京都調布市深大寺町 1,880
電話 武蔵野三鷹 (0422)47-5911 (大代表)

印刷所 株式会社 東京プレス
東京都板橋区桜川 2 丁目 27 の 12

Published by
NATIONAL AEROSPACE LABORATORY
1,880 Jindaiji, Chōfu, Tokyo
JAPAN